ORIGINAL PAPER

# Abnormal Corpus Callosum Connectivity, Socio-communicative Deficits, and Motor Deficits in Children with Autism Spectrum Disorder: A Diffusion Tensor Imaging Study

Ryuzo Hanaie · Ikuko Mohri · Kuriko Kagitani-Shimono ·
Masaya Tachibana · Junko Matsuzaki · Yoshiyuki Watanabe ·
Norihiko Fujita · Masako Taniike

**Abstract** In addition to social and communicative deficits, many studies have reported motor deficits in autism spectrum disorder (ASD). This study investigated the macro and microstructural properties of the corpus callosum (CC) of 18 children with ASD and 12 typically developing controls using diffusion tensor imaging tractography. We aimed to explore whether abnormalities of the CC were related to motor deficits, as well as social and communication deficits in children with ASD. The ASD group displayed abnormal macro and microstructure of the total CC and its subdivisions and its structural properties were related to socio-communicative deficits, but not to motor deficits in ASD. These findings advance our understanding of the contributions of the CC to ASD symptoms.

## Introduction

Autism spectrum disorder (ASD) is a complex group of neurodevelopmental disorders characterized by deficits in social interaction and verbal and nonverbal communication, as well as restricted, repetitive interests (American Psychiatric Association 2000). In addition to these core features, many studies have reported that motor deficits are common in patients with ASD (Fournier et al. 2010). Motor deficits may be related to the core features of ASD and contribute to difficulties in daily living skills (Jasmin et al. 2009; Leary and Hill 1996). However, like the core features of ASD, the brain mechanisms underlying motor deficits remain unknown.

A growing body of evidence suggests that the symptoms of ASD are related to altered connectivity between diverse cortical regions (Minshew and Williams 2007). One of the most effective and noninvasive methods for studying neural structural connectivity is diffusion tensor imaging (DTI). Several quantitative measurements, such as fractional anisotropy (FA), axial diffusivity (AD), and radial diffusivity (RD), are derived from DTI data. Although relationships between these indices and microstructural tissue properties are complex, FA is considered to be closely associated with myelination, axon diameter, fiber density, and fiber coherence, representing a measure of microstructural integrity of the white matter (WM) (Tournier et al. 2011). Human and animal studies have suggested that AD is related to axonal integrity, and that changes in RD are sensitive to alterations of myelination (Budde et al.

R. Hanaie · I. Mohri · K. Kagitani-Shimono · M. Tachibana ·
M. Taniike (✉)
Division of Developmental Neuroscience, United Graduate
School of Child Development, Osaka University, 2-2
Yamadaoka, Suita, Osaka 565-0871, Japan
e-mail: masako@kokoro.med.osaka-u.ac.jp

I. Mohri · J. Matsuzaki · M. Taniike
Molecular Research Center for Children's Mental Development,
United Graduate School of Child Development, Osaka
University, 2-2 Yamadaoka, Suita, Osaka 565-0871, Japan

I. Mohri · K. Kagitani-Shimono · M. Tachibana · M. Taniike
Department of Pediatrics, Osaka University Graduate School of
Medicine, 2-2 Yamadaoka, Suita, Osaka 565-0871, Japan

Y. Watanabe · N. Fujita
Department of Diagnostic and Interventional Radiology, Osaka
University Graduate School of Medicine, 2-2 Yamadaoka, Suita,
Osaka 565-0871, Japan

2009; Song et al. 2003). Using these parameters, many DTI studies have reported abnormalities in the microstructure of WM tracts in patients with ASD as compared to healthy controls (Travers et al. 2012).

Among WM tracts, the corpus callosum (CC) has been reported to be one of the most commonly affected WM tracts in patients with ASD (Aoki et al. 2013). Structural magnetic resonance imaging (MRI) studies have found a significant reduction in volume of the total CC (Hardan et al. 2009b; Keary et al. 2009), rostrum (Keary et al. 2009), genu (Keary et al. 2009; Vidal et al. 2006), body (Hardan et al. 2009b; Keary et al. 2009), isthmus (Freitag et al. 2009; Waiter et al. 2005) and splenium (Hardan et al. 2009b; Vidal et al. 2006; Waiter et al. 2005) in patients with ASD compared to healthy controls. In addition, a reduced FA and AD, and an increased RD of the total CC and its subdivisions in patients with ASD have been reported using several DTI techniques, such as voxel-based morphometry (VBM) (Barnea-Goraly et al. 2004), tract-based spatial statistics (TBSS) (Bakhtiari et al. 2012), and region-of-interest (ROI) analyses (Shukla et al. 2010). DTI tractography in patients with ASD also disclosed abnormal macrostructure, such as reduced tract volume (Thomas et al. 2011) and longer fiber length (Kumar et al. 2010) of the CC.

The CC is the largest fiber bundle in the human brain, connecting the two cerebral hemispheres homotopically or heterotopically. It serves as both an excitatory and inhibitory modulator of interhemispheric communication (Bloom and Hynd 2005). Because of its extensive connectivity, the correlation between structural changes in the CC and various brain functions including socio-communicative and motor functions has been investigated. For instance, a volumetric MRI study found that in patients with ASD, there is a relationship between the volume of CC subdivisions and social algorithm scores on the Autism Diagnostic Observation Schedule-Generic (ADOS-G) (Prigge et al. 2013). One DTI tractography study revealed a correlation between fiber length and density of the total CC and communication scores on the Vineland Adaptive Behavior Scales (VABS) (Kumar et al. 2010). In addition, social and communication deficits, which are core symptoms of ASD, have also been reported in patients with agenesis of the CC (AgCC) (Lau et al. 2013). Studies of patients with AgCC, acquired CC damage, and preterm-born children have suggested that abnormalities of the CC contribute to various motor deficits, including disturbances in uni- and bi-manual movement (Beaule et al. 2012; Eliassen et al. 2000), eye–hand coordination (Rademaker et al. 2004), balance (Moes et al. 2009), and gait (de Laat et al. 2011), which have also been found in patients with ASD (Glazebrook et al. 2009; Jansiewicz et al. 2006; Minshew et al. 2004; Rinehart et al. 2006).

These lines of evidence imply that abnormalities in CC connectivity are related to not only socio-communicative, but also motor deficits in ASD. However, to the best of our knowledge, there have been no studies investigating the relationships between abnormalities in CC connectivity and motor deficits in ASD by neuroimaging analysis. Since motor deficits are also related to difficulties in daily living skills in ASD children, clarification of the brain mechanisms underlying motor deficits is crucial for improving daily living skills and the quality of life in children with ASD.

The aim of the present study was to examine the macro and microstructural properties of the total CC and its subdivisions in children with ASD using DTI tractography and to compare these results to those of typically developing (TD) controls. We used DTI tractography and subdivided the total CC into the forceps minor (F-Mi), body, forceps major (F-Ma), and tapetum. Furthermore, we examined whether the macro and microstructural properties of subdivisions of the CC are related to motor deficits and socio-communicative deficits in children with ASD. We hypothesized that children with ASD would show significant abnormalities in the CC. Since the CC body connects the bilateral cortical regions involved in motor planning and execution (Hofer and Frahm 2006; Park et al. 2008), we hypothesized that macro and microstructural properties of the CC body would be related to motor deficits. In addition, since the F-Mi, F-Ma, and tapetum connect the bilateral cortical regions involved in social and communicative functions (Hofer and Frahm 2006; Park et al. 2008), we hypothesized that the macro and microstructural properties of the F-Mi, F-Ma, and tapetum would be related to socio-communicative deficits.

## Methods

### Participants

Eighteen children diagnosed with ASD (17 male and 1 female; mean age 9.5 ± 2.6 years; range 5–14 years) and 12 TD children (11 male and 1 female; mean age 10.8 ± 2.1 years; range 7–13 years) participated in this study. The diagnosis of ASD was made using criteria from the Diagnostic and Statistical Manual of Mental Disorders, Fourth Edition, Text Revision, and was further confirmed by the ADOS-G (Lord et al. 2000). To confirm the non-autistic traits of TD children, the Japanese version of the Autism Screening Questionnaire (ASQ-J) was used. None of the TD children had a history of learning, developmental, or neurological problems. According to the Edinburgh Handedness Inventory (Oldfield 1971), all participants were right-handed. Intelligence was evaluated

using the Wechsler Intelligence Scale for Children, Third Edition (WISC-III) for all but 2 ASD participants, for whom the Kaufman Assessment Battery for Children (K-ABC) was used. The WISC-III contains several subtests that provide scores for Verbal Intelligence Quotient (VIQ), Performance Intelligence Quotient (PIQ), and Full Scale Intelligence Quotient (FSIQ).

We chose a FSIQ threshold of ≥80 to ensure normal intelligence and minimize the effect of IQ on motor assessment. In addition, children with clinical seizures, or secondary ASD associated with genetic disorders were excluded from this study. Two patients with ASD were taking either methylphenidate or atomoxetine. In order to acquire MRI data, sedation was required in three children with ASD.

This study was approved by the Institutional Review Board and written informed consent was obtained from the parents of all participants.

## Motor Assessment

Motor function of the participants was assessed using the Movement Assessment Battery for Children 2 (M-ABC 2) (Henderson et al. 2007). The M-ABC 2 includes 8 subtests, which assess 3 components of motor function: manual dexterity, ball skills, and static and dynamic balance. In addition, the total test score was obtained. These scores can be presented as standard scores and percentiles. Standard scores range from 1 to 19, with higher scores indicative of better motor function. This test has 3 age ranges: 3–6, 7–10, and 11–16 years. Previous studies have found significant differences in motor function between children with ASD and TD children using the M-ABC 2 (Johnson et al. 2012; Whyatt and Craig 2012).

## MRI Acquisition

All images were acquired on a 3-Tesla GE MR system (Signa Excite HDxt; GE Healthcare, Milwaukee, USA). A three-dimensional (3D) $T_1$-weighted axial protocol was used for volumetric measurements of the total brain. Imaging parameters for 3D-$T_1$-weighted images were as follows: 3D-spoiled gradient recalled acquisition in steady state sequence, repetition time (TR) = 10.1 ms; echo time (TE) = 3.0 ms; flip angle = 18°; field of view (FOV) = 220 × 220 mm²; matrix size = 320 × 256; slice thickness = 1.4 mm; number of slices = 128; number of excitations (NEX) = 1.

DTI was performed using a single-shot spin-echo echo-planar imaging with sensitivity encoding parallel imaging (factor = 2) in the axial plane with 6 noncollinear directions. Imaging parameters were as follows: TR = 12,000 ms; TE = 86 ms; FOV = 260 × 260 mm²;

matrix size = 128 × 128; slice thickness = 3 mm; slice gap = 0; number of slices = 45–48; NEX = 1; and diffusion-weighting factor b = 800 and 0 s/mm². Foam pillows and cushions were used to minimize participants' head movement during scanning.

## Volumetric Analysis

Total brain volume (TBV) was analyzed using the software ANALYSE 8.1 (Mayo Clinic, MN). Automated and manual segmentation techniques were used. TBV was defined as total intracranial volume including all brain tissue and cerebrospinal fluid. All analyses were performed by a single rater blinded to diagnosis.

## DTI data Analysis

### Correction for Image Distortions

To correct for image distortions produced by eddy currents and head movement, the Automatic Image Registration (AIR) program was used. Diffusion-weighted images were realigned to the b = 0 image using a 12-parameter affine registration.

### Tractography Approach

DtiStudio (www.mristudio.org) was used for the tensor calculations and tractography. Tractography was performed on the basis of the Fiber Assignment by Continuous Tracking (FACT) method (Mori et al. 1999). To reconstruct the fibers of the CC, the FA and turning angle thresholds for the termination of fiber tracking were set to 0.20 and 60°, respectively. Initially, tracking was performed from all pixels inside the brain using the brute-force approach; subsequently, a multiple-ROI approach was used to reconstruct all tracts of interest (Huang et al. 2004). Although DtiStudio has some operations for a multiple-ROI approach, we chose the "OR," "AND," and "NOT" operations (Wakana et al. 2007). Fibers were reconstructed if they passed through the 2 ROIs (the "OR" and "AND" operations). Some fibers that appeared to track an error course were excluded with the "NOT" operation. The fibers of the CC were reconstructed by protocols based on previous publications (Huang et al. 2005; Thomas et al. 2011). ROI locations and reconstructed tracts are shown in Fig. 1. To reconstruct the F-Mi, the genu of the CC was defined as ROI 1 in the midsagittal plane, and ROI 2 was placed in the coronal plane anterior to the genu of the CC. To reconstruct the body, the body of the CC was defined as ROI 1 in the midsagittal plane, and ROI 2 was placed at the semioval center in the axial plane superior to the body of the CC. To reconstruct the F-Ma, the splenium of the CC was defined as ROI 1 in the midsagittal plane, and
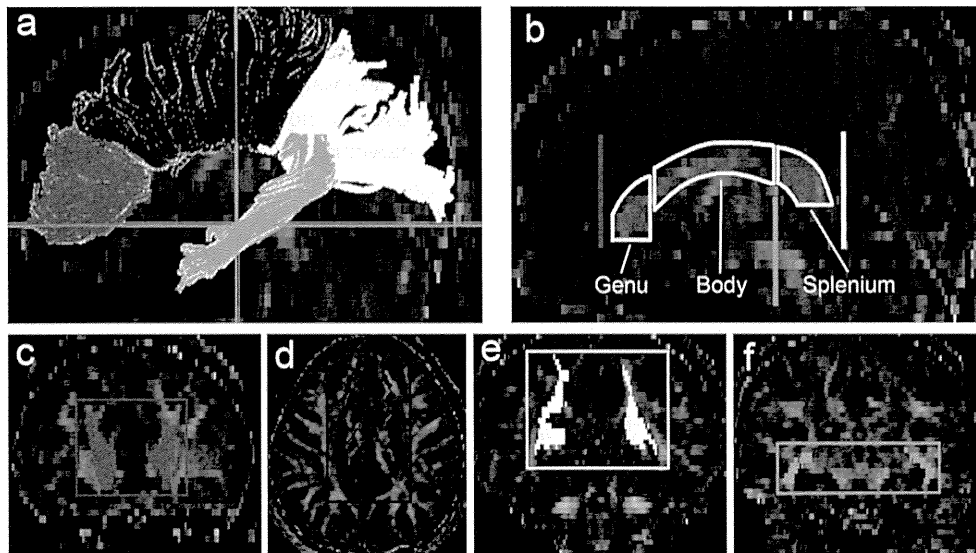
**Fig. 1** Region of interest (ROI) locations used for the reconstruction of the corpus callosum and its subdivisions. Reconstructed tracts are shown in (**a**): the forceps minor (F-Mi) = *red*; the body = *blue*; the forceps major (F-Ma) = *yellow*; the tapetum = *orange*. ROI 1 s are depicted by white lines in the sagittal plane (**b**). The genu and body were defined as ROI 1 for reconstructing the F-Mi and body, respectively. The splenium was defined as ROI 1 for both the F-Ma and tapetum. Vertical and horizontal color lines in the sagittal plane indicate slice levels where ROI 2 s were placed (**b**). ROI 2 s are depicted by *rectangular shapes* with *colored lines* in the coronal and axial planes (**c–f**). The *red rectangular shape* is ROI 2 for reconstructing the F-Mi (**c**), *blue* is for the body (**d**), *yellow* is for the F-Ma (**e**), and *orange* is for the tapetum (**f**) (Color figure online)

ROI 2 was placed in the coronal plane posterior to the splenium of the CC. To reconstruct the tapetum, the splenium of the CC was defined as ROI 1 in the midsagittal plane, and ROI 2 was placed in the coronal plane anterior to the splenium of the CC. All ROIs were placed on the color-coded map. The F-Mi, body, F-Ma, and tapetum were combined to reconstruct the entire CC. Tractography was performed by one rater (R.H.) who was completely blinded to participants' diagnoses. As the macrostructural properties of the tracts, tract volume (TV), fiber density (FD), and average fiber length (AFL) were calculated. In addition, the microstructural properties of the tracts including FA, AD, and RD were calculated. It should be cautioned that the terms "tract volume," "fiber density," and "average fiber length" used in current DTI studies do not denote the actual tract volume, fiber density, or length (Jones et al. 2013). These indices depend on the FA and angle threshold.

### Estimation for Head Movement

Since a recent study suggested that significant differences in head movement between two groups can affect the results of group comparisons of DTI outcomes (Yendiki et al. 2013), estimation for head movement was performed using SPM 8 (http://www.fil.ion.ucl.ac.uk/spm) and an in-house program created with Matlab R2013a (Math Works, Natick, MA, USA). The extent of the displacement of three translational components (x, y, z direction) between the first volume (b = 0 image) and each subsequent volume were calculated and these parameters were summed and averaged for each participant. In addition, the extent of the displacement of 3 rotational components (pitch, roll, yaw) between the first volume and each subsequent volume were calculated and the absolute value of these parameters were summed and averaged for each participant. A statistical comparison of head movement between the two groups was performed.

### Statistical Analysis

Statistical analyses were performed using SPSS (IBM Inc., Tokyo, Japan). Independent sample *t*-tests were used to compare age, IQ, handedness, M-ABC 2 outcomes, TBV, and head movement between ASD and controls. Inter-group differences in the macro and microstructural properties of the total CC and its subdivisions were analyzed with analysis of variance (ANOVA). Because sedation might be related to head movement differences between the two groups and may have impacted the results, an ANOVA was also performed after removing the three sedated participants. In addition, analysis of covariance (ANCOVA) was applied to compare the CC measurements between the two groups while controlling for confounding factors such as TBV, age, and FSIQ. Furthermore, within each group, Pearson's correlation coefficients were used to investigate the relationships between the measurements of the CC body and motor function. Correlation analyses were performed between the measurements of the CC body and the component scores for manual dexterity, ball skills, balance, and the total test score

**Table 1** Demographic characteristics of the participants

| | ASD (n = 18) | | TD (n = 12) | | p value |
|---|---|---|---|---|---|
| | Mean | SD | Mean | SD | |
| Age (years) | 9.5 | 2.6 | 10.8 | 2.1 | 0.145 |
| FSIQ[a] | 102.1 | 11.1 | 112.5 | 11.3 | 0.018* |
| VIQ[a] | 102.9 | 15.6 | 111.3 | 16.6 | 0.168 |
| PIQ[a] | 100.7 | 10.5 | 110.9 | 7.4 | 0.007** |
| Handedness | 91.7 | 17.5 | 93.3 | 20.2 | 0.820 |
| *ADOS-G subscales* | | | | | |
| Communication | 3.4 | 1.4 | | | |
| Reciprocal social interaction | 7.2 | 2.4 | | | |
| ASQ-J | | | 2.6 | 3.9 | |

*ASD* autism spectrum disorders, *TD* typically developing controls, *FSIQ* Full Scale Intelligence Quotient, *VIQ* Verbal Intelligence Quotient, *PIQ* Performance Intelligence Quotient, *ADOS-G* Autism Diagnostic Observation Schedule-Generic, *ASQ-J* Japanese version of the Autism Screening Questionnaire (cut-off ≥13), *SD* standard deviation

* Significance level set at 0.05

** Significance level set at 0.01

[a] Scores for the mental processing composite, the sequential processing scale, and the simultaneous processing scale in The Kaufman Assessment Battery for Children were entered into the FSIQ, VIQ, and PIQ, respectively, for 2 ASD participants

on the M-ABC 2. In addition, correlation analyses were performed between the measurements of the F-Mi, F-Ma, and tapetum and scores for communication and reciprocal social interaction on the ADOS-G within the ASD group using Spearman's correlation coefficients, since scores on the ADOS-G were not normally distributed. Because different ADOS-G modules were used across participants (the number of participants; module 1 = 1, module 2 = 5, module 3 = 12), correlation analyses between the measurements of the F-Mi, F-Ma, and tapetum and the ADOS-G scores were performed only in participants who were administered module 3. When there was a significant correlation between 2 variables, the same analysis was repeated after covarying for FSIQ and age. To correct for multiple comparisons, a false discovery rate (FDR) procedure was performed at a q value = 0.05 (Benjamini and Hochberg 1995).

## Results

### Demographics

As shown in Table 1, there were no significant differences between the two groups in age, VIQ, and handedness. However, there were significant differences between the two groups in FSIQ and PIQ. The ASD group showed a

**Table 2** Scores for the movement assessment battery for children 2 (M-ABC 2)

| | ASD (n = 18) | | | TD (n = 12) | | | p value |
|---|---|---|---|---|---|---|---|
| | Mean | SD | Range | Mean | SD | Range | |
| Manual dexterity | 10.7 | 2.9 | 3–15 | 13.4 | 3.3 | 9–19 | 0.025* |
| Ball skills | 9.0 | 3.4 | 3–15 | 12.8 | 2.3 | 8–16 | 0.003** |
| Static and dynamic balance | 10.8 | 3.1 | 4–15 | 13.0 | 1.7 | 10–15 | 0.038* |
| Total test score | 10.3 | 3.0 | 5–16 | 14.3 | 2.7 | 11–19 | 0.001** |

*ASD* autism spectrum disorders, *TD* typically developing controls, *SD* standard deviation

* Significance level set at 0.05

** Significance level set at 0.01

lower score than the TD group in FSIQ and PIQ ($p = 0.018$, $p = 0.007$, respectively).

### Group Differences in Motor Function

As shown in Table 2, the ASD group had poorer motor function than the TD group (total test score; $p = 0.001$). The ASD group showed significant impairment in manual dexterity ($p = 0.025$), ball skills ($p = 0.003$), and static and dynamic balance ($p = 0.038$).

### Group Differences in TBV

There was no significant difference between the ASD group (1,443 ± 113 mL) and the TD group (1,472 ± 108 mL) in TBV ($p = 0.516$).

### Group Differences in Head Movement

There were no significant differences between the two groups in translation (ASD group = 0.61 ± 0.24 mm, TD group = 0.46 ± 0.18 mm, $p = 0.075$, d = 0.71) or rotation (ASD group = 0.24 ± 0.13°, TD group = 0.17 ± 0.09°, $p = 0.120$, d = 0.64). However, since the difference in translation between the two groups showed a trend towards significance and had a medium effect size, translation was included in the ANCOVA.

### Group Differences in DTI Outcome Measurements

#### ANOVA Results

The ANOVA revealed that the ASD group had a significantly decreased TV in the total CC [$F(1,28) = 4.765$, $p = 0.038$], body [$F(1,28) = 4.899$, $p = 0.035$], and F-Ma

**Table 3** Tract volume, fiber density, and average fiber length of the total corpus callosum and its subdivisions

| | ASD (n = 18) | | TD (n = 12) | | ANOVA | | ANCOVA[a] | | ANCOVA[b] | | ANCOVA[c] | | ANCOVA[d] | |
|---|---|---|---|---|---|---|---|---|---|---|---|---|---|---|
| | Mean | SD | Mean | SD | F | p value | F | p value | F | p value | F | p value | F | p value |
| *Tract volume (voxels)* | | | | | | | | | | | | | | |
| F-Mi | 6,104 | 1,461 | 6,583 | 840 | 1.048 | 0.315 | 0.566 | 0.459 | 0.753 | 0.393 | 1.335 | 0.258 | 0.058 | 0.812 |
| Body | 9,565 | 2,569 | 11,507 | 1,977 | 4.899 | 0.035* | 4.225 | 0.050 | 3.046 | 0.092 | 5.474 | 0.027* | 0.571 | 0.456 |
| F-Ma | 7,843 | 2,191 | 9,481 | 1,257 | 5.460 | 0.027* | 4.837 | 0.037* | 2.962 | 0.097 | 5.469 | 0.027* | 1.403 | 0.247 |
| Tapetum | 3,424 | 1,362 | 3,483 | 1,911 | 0.010 | 0.920 | 0.001 | 0.977 | 0.515 | 0.479 | 0.030 | 0.863 | 0.002 | 0.964 |
| Total CC | 25,280 | 5,003 | 28,877 | 3,329 | 4.765 | 0.038* | 4.363 | 0.046* | 2.376 | 0.135 | 5.539 | 0.026* | 0.610 | 0.442 |
| *Fiber density (fibers/voxel)* | | | | | | | | | | | | | | |
| F-Mi | 40.7 | 4.6 | 42.2 | 3.8 | 0.836 | 0.368 | 0.504 | 0.484 | 0.958 | 0.336 | 1.371 | 0.252 | 0.797 | 0.380 |
| Body | 18.8 | 5.3 | 22.1 | 4.6 | 3.240 | 0.083 | 2.701 | 0.112 | 2.638 | 0.116 | 3.691 | 0.065 | 0.328 | 0.571 |
| F-Ma | 47.4 | 22.4 | 54.1 | 18.7 | 0.723 | 0.402 | 0.521 | 0.477 | 0.077 | 0.783 | 0.781 | 0.385 | 0.037 | 0.850 |
| Tapetum | 19.3 | 11.3 | 20.4 | 12.0 | 0.075 | 0.786 | 0.056 | 0.814 | 0.516 | 0.479 | 0.173 | 0.681 | 0.039 | 0.845 |
| Total CC | 35.0 | 9.3 | 39.1 | 6.5 | 1.716 | 0.201 | 1.322 | 0.260 | 0.531 | 0.472 | 1.842 | 0.186 | 0.184 | 0.671 |
| *Average fiber length (mm)* | | | | | | | | | | | | | | |
| F-Mi | 85.4 | 6.3 | 88.2 | 4.2 | 1.819 | 0.188 | 1.263 | 0.271 | 1.872 | 0.182 | 3.173 | 0.086 | 0.688 | 0.414 |
| Body | 75.2 | 9.5 | 80.2 | 9.3 | 1.990 | 0.169 | 1.446 | 0.240 | 1.405 | 0.246 | 2.898 | 0.100 | 0.004 | 0.953 |
| F-Ma | 105.8 | 7.8 | 113.5 | 6.0 | 8.233 | 0.008** | 8.284 | 0.008** | 5.628 | 0.025* | 12.325 | 0.002** | 3.502 | 0.072 |
| Tapetum | 128.9 | 10.7 | 132.4 | 19.2 | 0.393 | 0.536 | 0.276 | 0.603 | 0.010 | 0.919 | 0.580 | 0.453 | 0.004 | 0.951 |
| Total CC | 93.1 | 6.3 | 98.3 | 4.7 | 5.927 | 0.022* | 5.826 | 0.023* | 3.336 | 0.079 | 9.836 | 0.004** | 1.500 | 0.231 |

Fiber density is obtained by determining the mean number of fibers passing through each voxel

*ASD* autism spectrum disorders, *TD* typically developing controls, *SD* standard deviation, *F-Mi* forceps minor, *F-Ma* forceps major, *Total CC* total corpus callosum, *ANOVA* analysis of variance, *ANCOVA* analysis of covariance

Tract volume is expressed as the number of voxels through which fibers pass

* Significance level set at 0.05. ** Significant after controlling for multiple comparisons by false discovery rate procedure

[a] ANCOVA completed using total brain volume as a covariate

[b] ANCOVA completed using age as a covariate

[c] ANCOVA completed using translation as a covariate

[d] ANCOVA completed using FSIQ as a covariate

$[F(1,28) = 5.460, p = 0.027]$, as well as significantly shorter AFL in the total CC $[F(1,28) = 5.927, p = 0.022]$ and F-Ma $[F(1,28) = 8.233, p = 0.008]$ compared to the TD group (Table 3). In addition, the ASD group had a significantly lower AD than the TD group in the tapetum $[F(1,28) = 5.301, p = 0.029]$ (Table 4). ANOVAs for FA, RD, and FD did not reveal any significant differences between the two groups (Tables 3 and 4). The AFL differences between the two groups in the F-Ma remained significant after correcting for multiple comparisons. Even after excluding the three sedated participants, the ANOVA revealed similar results as follows: the ASD group had a significantly decreased TV in the body $[F(1,25) = 4.887, p = 0.036]$, and F-Ma $[F(1,25) = 5.500, p = 0.027]$, as well as a shorter AFL in the total CC $[F(1,25) = 5.184, p = 0.032]$ and F-Ma $[F(1,25) = 8.781, p = 0.007]$ compared to the TD group. The differences between the two groups in the TV of the total CC $[F(1,25) = 3.963, p = 0.058]$ and AD of the tapetum $[F(1,25) = 4.154, p = 0.052]$ showed a trend towards significance.

### ANCOVA Results

After covarying for TBV, the ASD group had a significantly decreased TV in the total CC $[F(1,27) = 4.363, p = 0.046]$, and F-Ma $[F(1,27) = 4.837, p = 0.037]$, as well as a shorter AFL in the total CC $[F(1,27) = 5.826, p = 0.023]$ and F-Ma $[F(1,27) = 8.284, p = 0.008]$ compared to the TD group (Table 3). In addition, the ASD group had a significantly lower AD than the TD group in the tapetum $[F(1,27) = 4.650, p = 0.040]$ (Table 4). The AFL differences between the two groups in the F-Ma remained significant after correcting for multiple comparisons. After covarying for age, the ASD group had a significantly shorter AFL in the F-Ma $[F(1,27) = 5.628, p = 0.025]$ and lower AD in the tapetum $[F(1,27) = 4.738, p = 0.038]$ compared to the TD group (Tables 3 and 4). These results did not remain significant after correcting for multiple comparisons. In addition, after covarying for translation, the ASD group had a significantly decreased TV in the total CC $[F(1,27) = 5.539, p = 0.026]$, body $[F(1,27) = 5.474,$

**Table 4** Fractional anisotropy, axial diffusivity, and radial diffusivity of the total corpus callosum and its subdivisions

| | ASD (n = 18) | | TD (n = 12) | | ANOVA | | ANCOVA[a] | | ANCOVA[b] | | ANCOVA[c] | | ANCOVA[d] | |
|---|---|---|---|---|---|---|---|---|---|---|---|---|---|---|
| | Mean | SD | Mean | SD | F | p value | F | p value | F | p value | F | p value | F | p value |
| *Fractional anisotropy* | | | | | | | | | | | | | | |
| F-Mi | 0.57 | 0.02 | 0.57 | 0.01 | 0.137 | 0.714 | 0.808 | 0.779 | 0.297 | 0.590 | 0.006 | 0.938 | 0.977 | 0.332 |
| Body | 0.53 | 0.03 | 0.54 | 0.02 | 0.921 | 0.345 | 0.632 | 0.433 | 0.145 | 0.707 | 0.459 | 0.504 | 0.431 | 0.517 |
| F-Ma | 0.61 | 0.02 | 0.62 | 0.02 | 0.229 | 0.636 | 0.129 | 0.722 | 0.066 | 0.799 | 0.263 | 0.612 | 0.191 | 0.666 |
| Tapetum | 0.58 | 0.02 | 0.58 | 0.02 | 0.032 | 0.859 | 0.009 | 0.926 | 0.013 | 0.911 | 0.380 | 0.543 | 0.755 | 0.393 |
| Total CC | 0.58 | 0.02 | 0.59 | 0.02 | 0.722 | 0.403 | 0.494 | 0.488 | 0.022 | 0.884 | 0.557 | 0.462 | 0.136 | 0.715 |
| *Axial diffusivity* | | | | | | | | | | | | | | |
| F-Mi | 1.57 | 0.04 | 1.58 | 0.04 | 1.061 | 0.312 | 0.937 | 0.342 | 1.213 | 0.281 | 0.658 | 0.424 | 0.188 | 0.668 |
| Body | 1.52 | 0.05 | 1.53 | 0.04 | 0.474 | 0.497 | 0.238 | 0.629 | 1.045 | 0.316 | 0.530 | 0.473 | 0.207 | 0.653 |
| F-Ma | 1.58 | 0.07 | 1.60 | 0.05 | 0.821 | 0.373 | 0.536 | 0.470 | 0.890 | 0.354 | 0.623 | 0.437 | 0.541 | 0.469 |
| Tapetum | 1.58 | 0.07 | 1.64 | 0.07 | 5.301 | 0.029* | 4.650 | 0.040* | 4.738 | 0.038* | 4.128 | 0.052 | 3.638 | 0.067 |
| Total CC | 1.57 | 0.05 | 1.58 | 0.04 | 1.244 | 0.274 | 0.903 | 0.350 | 1.415 | 0.245 | 0.959 | 0.336 | 0.820 | 0.373 |
| *Radial diffusivity* | | | | | | | | | | | | | | |
| F-Mi | 0.57 | 0.04 | 0.57 | 0.02 | 0.015 | 0.903 | 0.027 | 0.871 | 1.274 | 0.269 | 0.128 | 0.723 | 1.376 | 0.251 |
| Body | 0.61 | 0.04 | 0.60 | 0.03 | 1.014 | 0.323 | 0.868 | 0.360 | 0.123 | 0.728 | 0.514 | 0.480 | 0.152 | 0.700 |
| F-Ma | 0.51 | 0.03 | 0.51 | 0.02 | 0.159 | 0.693 | 0.165 | 0.688 | 0.133 | 0.718 | 0.155 | 0.697 | 0.286 | 0.597 |
| Tapetum | 0.56 | 0.03 | 0.58 | 0.05 | 1.961 | 0.172 | 2.411 | 0.132 | 2.809 | 0.160 | 0.768 | 0.389 | 3.589 | 0.069 |
| Total CC | 0.55 | 0.03 | 0.55 | 0.03 | 0.281 | 0.600 | 0.236 | 0.631 | 0.222 | 0.641 | 0.178 | 0.677 | 0.339 | 0.565 |

No units for fractional anisotropy. Units for axial diffusivity and radial diffusivity are $10^{-3}$ mm$^2$/s

*ASD* autism spectrum disorders, *TD* typically developing controls, *SD* standard deviation, *F-Mi* forceps minor; *F-Ma* forceps major, *Total CC* total corpus callosum, *ANOVA* analysis of variance, *ANCOVA* analysis of covariance

* Significance level set at 0.05

[a] ANCOVA completed using total brain volume as a covariate

[b] ANCOVA completed using age as a covariate

[c] ANCOVA completed using translation as a covariate

[d] ANCOVA completed using Full Scale Intelligence Quotient as a covariate

$p = 0.027$], and F-Ma [$F(1,27) = 5.469$, $p = 0.027$], as well as a shorter AFL in the total CC [$F(1,27) = 9.836$, $p = 0.004$] and F-Ma [$F(1,27) = 12.325$, $p = 0.002$] compared to the TD group (Table 3). The AFL differences between the two groups in the total CC and F-Ma remained significant after correcting for multiple comparisons. Covarying for FSIQ reduced the significance of all results. ANCOVAs for FA, RD, and FD did not reveal any significant differences between the two groups (Tables 3 and 4).

The Relationships Between DTI Outcome Measurements of the CC Body and Motor Function

Within the ASD group, there were no significant correlations between the macro and microstructural properties of the CC body and the test scores on the M-ABC 2 ($r = -0.257$–$0.391$; $p > 0.109$). In addition, within the TD group, there were no significant correlations between the macro and microstructural properties of the CC body and the test scores on the M-ABC 2 ($r = -0.503$–$0.264$; $p > 0.096$).

The Relationships Between DTI Outcome Measurements of the F-Mi, F-Ma, and Tapetum and the Severity of Socio-communicative Deficits

Within the ASD group, significant strong negative correlations were identified between the ADOS-G score for communication and the FA of the F-Ma ($r = -0.790$; $p = 0.002$; Fig. 2) or TV of the tapetum ($r = -0.622$; $p = 0.031$). Higher ADOS-G scores for communication were associated with lower FA of the F-Ma and smaller volume of the tapetum. A significant moderate negative correlation was also recognized between the ADOS-G score for reciprocal social interaction and the FD of the F-Mi ($r = -0.612$; $p = 0.034$). Higher ADOS-G scores for reciprocal social interaction were associated with lower FD of the F-Mi. A correlation between the ADOS-G score for communication and the FA of the F-Ma remained significant after covarying for FSIQ and age ($r = -0.789$; $p = 0.007$). In addition, this result remained significant after correcting for multiple comparisons.
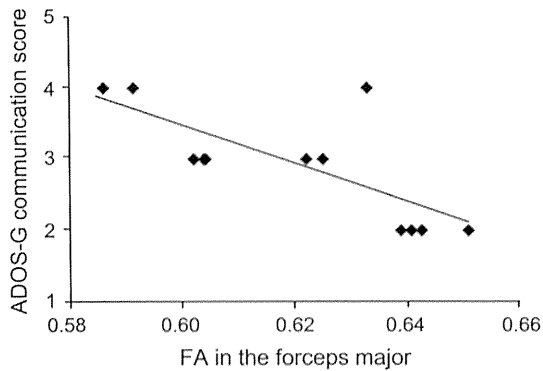
**Fig. 2** Scatter plot of correlation analysis in the autism spectrum disorder (ASD) group. There was a strong negative correlation between the score for communication on the Autism Diagnostic Observation Schedule-Generic (ADOS-G) and the fractional anisotropy (FA) of the forceps major (F-Ma) ($r = -0.790$; $p = 0.002$). Correlation analysis was performed using Spearman's correlation

## Discussion

This is the first study to investigate the relationships between CC connectivity abnormalities and motor deficits in children with ASD using DTI tractography. Furthermore, this is the first investigation to show that macro and microstructural properties of the CC were related to socio-communicative deficits, but not to motor deficits, in children with ASD. Especially, the AFL difference of the F-Ma between the ASD and TD groups, and the strong correlation between the ADOS-G score for communication and the FA of the F-Ma in the ASD group, were striking because they remained significant after controlling for confounding factors and multiple comparisons.

Although our findings of a decreased TV in the total CC, body, and F-Ma did not remain significant after correcting for multiple comparisons, they are consistent with the findings from previous volumetric and DTI studies (Freitag et al. 2009; Hardan et al. 2009b; Thomas et al. 2011; Waiter et al. 2005; Vidal et al. 2006). However, the results of our study are not consistent with a previous DTI tractography study regarding AFL. While we found that the ASD group had a significantly shorter AFL, the previous study reported a significantly longer AFL and higher FD of the CC in children with ASD (Kumar et al. 2010). Reasons for this inconsistency may be that the previous study recruited younger children with ASD than the current study, and it did not covariate for TBV. Since it is well known that there is an increase in brain size and abnormal maturation of the WM in younger children with ASD (Courchesne et al. 2001; Wolff et al. 2012), the findings of longer AFL and higher FD of the CC in the previous study may be related to these abnormalities. In addition, the ASD

group had a significantly lower AD in the tapetum in our study. Similarly, a lower AD in several fiber tracts including the CC was reported in previous DTI studies of patients with ASD (Cheng et al. 2010; Noriuchi et al. 2010; Shukla et al. 2010). Since AD has been suggested to be related to axonal integrity, the lower AD in the ASD group may reflect decreased axon diameter, or lack of fiber coherence (Schwartz et al. 2005; Wu et al. 2007).

The body of the CC connects bilateral cortical areas involved in motor planning and execution, such as the premotor, supplementary motor, primary motor, and sensory cortices (Hofer and Frahm 2006; Park et al. 2008). Furthermore, previous studies have suggested that the CC abnormalities contribute to various motor deficits as described. However, surprisingly, we could not find any correlations between motor function, which was evaluated with the M-ABC 2, and macro and microstructural properties of the CC body in the ASD group. This finding suggests that the CC abnormalities play a less important role in motor deficits in children with ASD. It is plausible that abnormalities of intrahemispheric connectivity, for example between the parietal cortex and the premotor cortex, are related to motor deficits much more than to interhemispheric connectivity (Mostofsky and Ewen 2011). Alternatively, it is possible that abnormalities of cortico-subcortical connectivity between the cerebral cortex and the cerebellum or basal ganglia mainly contribute to motor deficits in children with ASD (Mostofsky et al. 2009; Qiu et al. 2010). Indeed, a recent DTI tractography study has demonstrated that children with ASD and TD children have significant differences in the microstructure of the superior cerebellar peduncle, which is an efferent pathway of the cerebellum, and that this difference was related to motor deficits in children with ASD (Hanaie et al. 2013). However, the possibility that the CC contributes to motor deficits in children with ASD was not exclusively ruled out. First of all, a standardized test such as the M-ABC 2 may not be optimal for investigating the CC-related motor function, since a previous study suggested that interhemispheric communication via the CC may be related to task complexity (Clawson et al. 2013).

The results of the present study suggest that structural changes in the F-Mi, F-Ma, and tapetum contribute to socio-communicative deficits in children with ASD. The F-Ma consists of fibers connecting the bilateral parietal, occipital, and temporal regions, including the superior and inferior parietal lobules and fusiform gyrus (Pannek et al. 2010; Park et al. 2008). The superior and inferior parietal lobules play important roles in attention and language functions (Townsend et al. 1996; Heim et al. 2012; Vigneau et al. 2006), while the fusiform gyrus is involved in face processing (Haxby et al. 2000). The tapetum consists of fibers connecting the bilateral temporal lobes including the

superior temporal gyrus (STG), which is a crucial region for both language and social cognition (Pannek et al. 2010; Park et al. 2008; Redcay 2008; Vigneau et al. 2006; Hofer and Frahm 2006). Therefore, alteration in the F-Ma and tapetum may contribute to verbal and nonverbal communication deficits in children with ASD, which has been reported in previous studies (Corbett et al. 2009; Kjelgaard and Tager-Flusberg 2001; Williams et al. 2013). The F-Mi consists of fibers connecting the bilateral frontal regions, including the pars triangularis, medial prefrontal, and orbitofrontal cortex (Pannek et al. 2010; Park et al. 2008). It is well known that the pars triangularis is involved in language functions (Knaus et al. 2009). In addition, the medial prefrontal and orbitofrontal cortices play important roles in theory of mind (ToM) and empathy (Vollm et al. 2006). Therefore, alteration or developmental delay in the F-Mi may contribute to deficits in language, ToM, and empathy, which are important for social interaction, in patients with ASD (Kana et al. 2012; Vollm et al. 2006).

The CC is considered to have both inhibitory and excitatory influences on bilateral cortical areas through various conduction velocity channels of the callosal axon. Furthermore, it is believed that these inhibitory and excitatory influences are crucial for the organization of synchronous neural assemblies in the cortical areas, cerebral lateralization, and structural asymmetry (Bloom and Hynd 2005; Innocenti 2009). In this study, we found shorter AFL of the F-Ma and total CC, and lower AD in the tapetum, suggestive of axonal alteration. Since conduction velocity is associated with axonal length and diameter (Paus and Toro 2009; Zwarts and Guechev 1995), axonal abnormalities may affect conduction velocity, leading to an imbalance of inhibitory and excitatory influences of the CC on cortical regions. In turn, this imbalance may contribute to impaired cerebral lateralization and structural asymmetry of cortical regions that are involved in social and communicative functions. Indeed, previous studies have reported abnormalities of both cerebral lateralization and structural asymmetry of cortical regions that are connected through the F-Mi, F-Ma, or tapetum in patients with ASD (Cardinale et al. 2013; De Fosse et al. 2004; Gage et al. 2009; Herbert et al. 2002). On the other hand, abnormalities of the cortical areas may affect the CC volume and its fiber geometry. In one study investigating the direct correlation between the size of the CC and the gyral window, which refers to the space for afferent/efferent cortical connections, the authors hypothesized that a reduced gyral window biases toward shorter connecting fibers at the expense of longer connecting fibers (Casanova et al. 2009). Our findings of decreased TV and shorter AFL of the CC are consistent with this hypothesis.

Our study has several limitations. First, we included relatively small sample groups and only patients with high-functioning ASD; therefore, it is unknown whether our findings apply to patients with low-functioning ASD. Secondly, our sample groups were not matched for IQ. Although covarying for FSIQ made differences in the macro and microstructure of the CC less significant, arguments exist about whether covarying for FSIQ is suitable for the study of neurodevelopmental disorders, such as ASD (Dennis et al. 2009). Because limited cognitive functions are probably a part of the autistic features, controlling for IQ differences may eliminate a variability associated with ASD (Frazier et al. 2012; Hardan et al. 2009a). Third, we found abnormal indices of CC macrostructure, but abnormal indices of CC microstructure, such as FA and RD, were not observed except for AD. We used six noncollinear directions and NEX = 1 for DTI data acquisition, which met the minimal requirements, but were not optimal for diffusion tensor calculation (Tournier et al. 2011); it is generally recommended that the use of more than six directions provides a better estimate of DTI outcome, such as FA (Lebel et al. 2012). Although the rationale for our selection was that the time necessary for DTI acquisition should be as short as possible to avoid artifacts caused by movement, the minimum number of gradient directions may have impacted the estimation of DTI outcome, and may have made the FA and RD differences between the small sample groups difficult to detect. Alternatively, the presence of crossing fibers might be related to the lack of microstructural abnormalities. Previous studies suggested that regions with crossing fibers showed lower or higher FA (Douaud et al. 2011; Lebel et al. 2010). Since lateral projections of the CC cross the association fibers lateral to the CC, regions with mixed lower and higher FA might obscure true FA differences between small sample groups. Fourth, while the AFL of the CC has been investigated here and in previous studies, it is difficult to interpret the findings of abnormal fiber length. Since this index depends on the FA threshold value used to determine the endpoints of tracking, it is unclear whether it reflects actual fiber length. Our findings of shorter AFL mean that the FA threshold value reached the endpoints sooner in the ASD group than in the TD group. Although inter-group differences in overall FA were not observed, it is possible that the FA decreases at some tract regions because of axon and/or myelin abnormalities in the ASD group. A difference in the locations of those abnormalities may lead to different tracking endpoints. In addition, as stated above, the presence of crossing fibers might be related to shorter AFL. For instance, a shorter AFL might result from an increased crossing fiber volume in the ASD group than in the TD group. Such a situation might lower the FA value and increase the difficulty of fiber tracking in the ASD group in the lateral projections of the CC. As a result, the remaining reconstructed fibers could be shorter,

and would be calculated as having a shorter AFL. In the future, to clarify the possible effects of crossing fibers, tractography studies investigating all of the major fiber bundles that cross the CC are needed.

In summary, the present study revealed that children with ASD and TD children have significant differences in the macro and microstructure of the CC and that the structural properties of the CC are related to socio-communicative deficits, but not to motor deficits in ASD. Our findings improve the current knowledge regarding the mechanisms underlying socio-communicative and motor deficits and may help guide effective interventions in children with ASD.

# References

American Psychiatric Association. (2000). Diagnostic and statistical manual of mental disorders (4th ed. text revision). Washington, DC: American Psychiatric Association.

Aoki, Y., Abe, O., Nippashi, Y., & Yamasue, H. (2013). Comparison of white matter integrity between autism spectrum disorder subjects and typically developing individuals: A meta-analysis of diffusion tensor imaging tractography studies. *Molecular Autism*,. doi:10.1186/2040-2392-4-25.

Bakhtiari, R., Zürcher, N. R., Rogier, O., Russo, B., Hippolyte, L., Granziera, C., et al. (2012). Differences in white matter reflect atypical developmental trajectory in autism: A tract-based spatial statistics study. *NeuroImage (Amst)*,. doi:10.1016/j.nicl.2012.09.001.

Barnea-Goraly, N., Kwon, H., Menon, V., Eliez, S., Lotspeich, L., & Reiss, A. L. (2004). White matter structure in autism: Preliminary evidence from diffusion tensor imaging. *Biological Psychiatry, 55*, 323–326.

Beaule, V., Tremblay, S., & Theoret, H. (2012). Interhemispheric control of unilateral movement. *Neural Plasticity*,. doi:10.1155/2012/627816.

Benjamini, Y., & Hochberg, Y. (1995). Controlling the false discovery rate: A practical and powerful approach to multiple testing. *Journal of the Royal Statistical Society. Series B (Methodological), 57*, 289–300.

Bloom, J. S., & Hynd, G. W. (2005). The role of the corpus callosum in interhemispheric transfer of information: Excitation or inhibition? *Neuropsychology Review, 15*, 59–71.

Budde, M. D., Xie, M., Cross, A. H., & Song, S. K. (2009). Axial diffusivity is the primary correlate of axonal injury in the experimental autoimmune encephalomyelitis spinal cord: A quantitative pixelwise analysis. *Journal of Neuroscience, 29*, 2805–2813.

Cardinale, R. C., Shih, P., Fishman, I., Ford, L. M., & Muller, R. A. (2013). Pervasive rightward asymmetry shifts of functional networks in autism spectrum disorder. *JAMA Psychiatry*,. doi:10.1001/jamapsychiatry.2013.382.

Casanova, M. F., El-Baz, A., Mott, M., Mannheim, G., Hassan, H., Fahmi, R., et al. (2009). Reduced gyral window and corpus callosum size in autism: Possible macroscopic correlates of a minicolumnopathy. *Journal of Autism and Developmental Disorders, 39*, 751–764.

Cheng, Y., Chou, K. H., Chen, I. Y., Fan, Y. T., Decety, J., & Lin, C. P. (2010). Atypical development of white matter microstructure in adolescents with autism spectrum disorders. *Neuroimage, 50*, 873–882.

Clawson, A., Clayson, P. E., South, M., Bigler, E. D., & Larson, M. J. (2013). An electrophysiological investigation of interhemispheric transfer time in children and adolescents with high-functioning autism spectrum disorders. *Journal of Autism and Developmental Disorders*,. doi:10.1007/s10803-013-1895-7.

Corbett, B. A., Carmean, V., Ravizza, S., Wendelken, C., Henry, M. L., Carter, C., et al. (2009). A functional and structural study of emotion and face processing in children with autism. *Psychiatry Research, 173*, 196–205.

Courchesne, E., Karns, C. M., Davis, H. R., Ziccardi, R., Carper, R. A., Tigue, Z. D., et al. (2001). Unusual brain growth patterns in early life in patients with autistic disorder: An MRI study. *Neurology, 57*, 245–254.

De Fosse, L., Hodge, S. M., Makris, N., Kennedy, D. N., Caviness, V. S, Jr, McGrath, L., et al. (2004). Language-association cortex asymmetry in autism and specific language impairment. *Annals of Neurology, 56*, 757–766.

de Laat, K. F., Tuladhar, A. M., van Norden, A. G. W., Norris, D. G., Zwiers, M. P., & de Leeuw, F.-E. (2011). Loss of white matter integrity is associated with gait disorders in cerebral small vessel disease. *Brain, 134*, 73–83.

Dennis, M., Francis, D. J., Cirino, P. T., Schachar, R., Barnes, M. A., & Fletcher, J. M. (2009). Why IQ is not a covariate in cognitive studies of neurodevelopmental disorders. *Journal of the International Neuropsychological Society, 15*, 331–343.

Douaud, G., Jbabdi, S., Behrens, T. E., Menke, R. A., Gass, A., Monsch, A. U., et al. (2011). DTI measures in crossing-fibre areas: Increased diffusion anisotropy reveals early white matter alteration in MCI and mild Alzheimer's disease. *Neuroimage, 55*, 880–890.

Eliassen, J. C., Baynes, K., & Gazzaniga, M. S. (2000). Anterior and posterior callosal contributions to simultaneous bimanual movements of the hands and fingers. *Brain, 123*(Pt 12), 2501–2511.

Fournier, K. A., Hass, C. J., Naik, S. K., Lodha, N., & Cauraugh, J. H. (2010). Motor coordination in autism spectrum disorders: A synthesis and meta-analysis. *Journal of Autism and Developmental Disorders, 40*, 1227–1240.

Frazier, T. W., Keshavan, M. S., Minshew, N. J., & Hardan, A. Y. (2012). A two-year longitudinal MRI study of the corpus callosum in autism. *Journal of Autism and Developmental Disorders, 42*, 2312–2322.

Freitag, C. M., Luders, E., Hulst, H. E., Narr, K. L., Thompson, P. M., Toga, A. W., et al. (2009). Total brain volume and corpus callosum size in medication-naive adolescents and young adults with autism spectrum disorder. *Biological Psychiatry, 66*, 316–319.

Gage, N. M., Juranek, J., Filipek, P. A., Osann, K., Flodman, P., Isenberg, A. L., et al. (2009). Rightward hemispheric asymmetries in auditory language cortex in children with autistic disorder: An MRI investigation. *Journal of Neurodevelopmental Disorders, 1*, 205–214.

Glazebrook, C., Gonzalez, D., Hansen, S., & Elliott, D. (2009). The role of vision for online control of manual aiming movements in persons with autism spectrum disorders. *Autism, 13*, 411–433.

Hanaie, R., Mohri, I., Kagitani-Shimono, K., Tachibana, M., Azuma, J., Matsuzaki, J., et al. (2013). Altered microstructural connectivity of the superior cerebellar peduncle is related to motor

dysfunction in children with autistic spectrum disorders. *Cerebellum,.* doi:10.1007/s12311-013-0475-x.

Hardan, A. Y., Libove, R. A., Keshavan, M. S., Melhem, N. M., & Minshew, N. J. (2009a). A preliminary longitudinal magnetic resonance imaging study of brain volume and cortical thickness in autism. *Biological Psychiatry, 66*, 320–326.

Hardan, A. Y., Pabalan, M., Gupta, N., Bansal, R., Melhem, N. M., Fedorov, S., et al. (2009b). Corpus callosum volume in children with autism. *Psychiatry Research, 174*, 57–61.

Haxby, J. V., Hoffman, E. A., & Gobbini, M. I. (2000). The distributed human neural system for face perception. *Trends in Cognitive Sciences, 4*, 223–233.

Heim, S., Amunts, K., Hensel, T., Grande, M., Huber, W., Binkofski, F., et al. (2012). The role of human parietal area 7A as a link between sequencing in hand actions and in overt speech production. *Frontiers in Psychology,.* doi:10.3389/fpsyg.2012.00534.

Henderson, S., Sugden, D., & Barnett, A. L. (2007). *The movement assessment battery for children* (2nd ed.). London: The Psychological Corporation.

Herbert, M. R., Harris, G. J., Adrien, K. T., Ziegler, D. A., Makris, N., Kennedy, D. N., et al. (2002). Abnormal asymmetry in language association cortex in autism. *Annals of Neurology, 52*, 588–596.

Hofer, S., & Frahm, J. (2006). Topography of the human corpus callosum revisited—comprehensive fiber tractography using diffusion tensor magnetic resonance imaging. *Neuroimage, 32*, 989–994.

Huang, H., Zhang, J., Jiang, H., Wakana, S., Poetscher, L., Miller, M. I., et al. (2005). DTI tractography based parcellation of white matter: Application to the mid-sagittal morphology of corpus callosum. *Neuroimage, 26*, 195–205.

Huang, H., Zhang, J., van Zijl, P. C., & Mori, S. (2004). Analysis of noise effects on DTI-based tractography using the brute-force and multi-ROI approach. *Magnetic Resonance in Medicine, 52*, 559–565.

Innocenti, G. M. (2009). Dynamic interactions between the cerebral hemispheres. *Experimental Brain Research, 192*, 417–423.

Jansiewicz, E. M., Goldberg, M. C., Newschaffer, C. J., Denckla, M. B., Landa, R., & Mostofsky, S. H. (2006). Motor signs distinguish children with high functioning autism and Asperger's syndrome from controls. *Journal of Autism and Developmental Disorders, 36*, 613–621.

Jasmin, E., Couture, M., McKinley, P., Reid, G., Fombonne, E., & Gisel, E. (2009). Sensori-motor and daily living skills of preschool children with autism spectrum disorders. *Journal of Autism and Developmental Disorders, 39*, 231–241.

Johnson, B. P., Rinehart, N. J., Papadopoulos, N., Tonge, B., Millist, L., White, O., et al. (2012). A closer look at visually guided saccades in autism and Asperger's disorder. *Frontiers in Integrative Neuroscience,.* doi:10.3389/fnint.2012.00099.

Jones, D. K., Knosche, T. R., & Turner, R. (2013). White matter integrity, fiber count, and other fallacies: The do's and don'ts of diffusion MRI. *Neuroimage, 73*, 239–254.

Kana, R. K., Libero, L. E., Hu, C. P., Deshpande, H. D., & Colburn, J. S. (2012). Functional brain networks and white matter underlying theory-of-mind in autism. *Social Cognitive and Affective Neuroscience,.* doi:10.1093/scan/nss106.

Keary, C. J., Minshew, N. J., Bansal, R., Goradia, D., Fedorov, S., Keshavan, M. S., et al. (2009). Corpus callosum volume and neurocognition in autism. *Journal of Autism and Developmental Disorders, 39*, 834–841.

Kjelgaard, M. M., & Tager-Flusberg, H. (2001). An investigation of language impairment in autism: implications for genetic subgroups. *Language and Cognitive Processes, 16*, 287–308.

Knaus, T. A., Silver, A. M., Dominick, K. C., Schuring, M. D., Shaffer, N., Lindgren, K. A., et al. (2009). Age-related changes in the anatomy of language regions in autism spectrum disorder. *Brain Imaging and Behavior, 3*, 51–63.

Kumar, A., Sundaram, S. K., Sivaswamy, L., Behen, M. E., Makki, M. I., Ager, J., et al. (2010). Alterations in frontal lobe tracts and corpus callosum in young children with autism spectrum disorder. *Cerebral Cortex, 20*, 2103–2113.

Lau, Y. C., Hinkley, L. B., Bukshpun, P., Strominger, Z. A., Wakahiro, M. L., Baron-Cohen, S., et al. (2013). Autism traits in individuals with agenesis of the corpus callosum. *Journal of Autism and Developmental Disorders, 43*, 1106–1118.

Leary, M. R., & Hill, D. A. (1996). Moving on: Autism and movement disturbance. *Mental Retardation, 34*, 39–53.

Lebel, C., Benner, T., & Beaulieu, C. (2012). Six is enough? Comparison of diffusion parameters measured using six or more diffusion-encoding gradient directions with deterministic tractography. *Magnetic Resonance in Medicine, 68*, 474–483.

Lebel, C., Caverhill-Godkewitsch, S., & Beaulieu, C. (2010). Age-related regional variations of the corpus callosum identified by diffusion tensor tractography. *Neuroimage, 52*, 20–31.

Lord, C., Risi, S., Lambrecht, L., Cook, E. H, Jr, Leventhal, B. L., DiLavore, P. C., et al. (2000). The autism diagnostic observation schedule-generic: A standard measure of social and communication deficits associated with the spectrum of autism. *Journal of Autism and Developmental Disorders, 30*, 205–223.

Minshew, N. J., Sung, K., Jones, B. L., & Furman, J. M. (2004). Underdevelopment of the postural control system in autism. *Neurology, 63*, 2056–2061.

Minshew, N. J., & Williams, D. L. (2007). The new neurobiology of autism: Cortex, connectivity, and neuronal organization. *Archives of Neurology, 64*, 945–950.

Moes, P., Schilmoeller, K., & Schilmoeller, G. (2009). Physical, motor, sensory and developmental features associated with agenesis of the corpus callosum. *Child: Care, Health and Development, 35*, 656–672.

Mori, S., Crain, B. J., Chacko, V. P., & van Zijl, P. C. (1999). Three-dimensional tracking of axonal projections in the brain by magnetic resonance imaging. *Annals of Neurology, 45*, 265–269.

Mostofsky, S. H., & Ewen, J. B. (2011). Altered connectivity and action model formation in autism is autism. *Neuroscientist, 17*, 437–448.

Mostofsky, S. H., Powell, S. K., Simmonds, D. J., Goldberg, M. C., Caffo, B., & Pekar, J. J. (2009). Decreased connectivity and cerebellar activity in autism during motor task performance. *Brain, 132*, 2413–2425.

Noriuchi, M., Kikuchi, Y., Yoshiura, T., Kira, R., Shigeto, H., Hara, T., et al. (2010). Altered white matter fractional anisotropy and social impairment in children with autism spectrum disorder. *Brain Research, 1362*, 141–149.

Oldfield, R. C. (1971). The assessment and analysis of handedness: The Edinburgh inventory. *Neuropsychologia, 9*, 97–113.

Pannek, K., Mathias, J. L., Bigler, E. D., Brown, G., Taylor, J. D., & Rose, S. (2010). An automated strategy for the delineation and parcellation of commissural pathways suitable for clinical populations utilising high angular resolution diffusion imaging tractography. *Neuroimage, 50*, 1044–1053.

Park, H. J., Kim, J. J., Lee, S. K., Seok, J. H., Chun, J., Kim, D. I., et al. (2008). Corpus callosal connection mapping using cortical gray matter parcellation and DT-MRI. *Human Brain Mapping, 29*, 503–516.

Paus, T., & Toro, R. (2009). Could sex differences in white matter be explained by g ratio? *Frontiers in Neuroanatomy,.* doi:10.3389/neuro.05.014.2009.

Prigge, M. B., Lange, N., Bigler, E. D., Merkley, T. L., Neeley, E. S., Abildskov, T. J., et al. (2013). Corpus callosum area in children and adults with autism. *Research in Autism Spectrum Disorders, 7*, 221–234.

Qiu, A., Adler, M., Crocetti, D., Miller, M. I., & Mostofsky, S. H. (2010). Basal ganglia shapes predict social, communication, and motor dysfunctions in boys with autism spectrum disorder. *Journal of the American Academy of Child and Adolescent Psychiatry, 49*, 539–551.

Rademaker, K. J., Lam, J. N., Van Haastert, I. C., Uiterwaal, C. S., Lieftink, A. F., Groenendaal, F., et al. (2004). Larger corpus callosum size with better motor performance in prematurely born children. *Seminars in Perinatology, 28*, 279–287.

Redcay, E. (2008). The superior temporal sulcus performs a common function for social and speech perception: Implications for the emergence of autism. *Neuroscience and Biobehavioral Reviews, 32*, 123–142.

Rinehart, N. J., Tonge, B. J., Bradshaw, J. L., Iansek, R., Enticott, P. G., & McGinley, J. (2006). Gait function in high-functioning autism and Asperger's disorder: Evidence for basal-ganglia and cerebellar involvement? *European Child and Adolescent Psychiatry, 15*, 256–264.

Schwartz, E. D., Cooper, E. T., Fan, Y., Jawad, A. F., Chin, C. L., Nissanov, J., et al. (2005). MRI diffusion coefficients in spinal cord correlate with axon morphometry. *NeuroReport, 16*, 73–76.

Shukla, D. K., Keehn, B., Lincoln, A. J., & Muller, R. A. (2010). White matter compromise of callosal and subcortical fiber tracts in children with autism spectrum disorder: A diffusion tensor imaging study. *Journal of the American Academy of Child and Adolescent Psychiatry, 49*, 1269–1278., 1278 e1261–e1262.

Song, S. K., Sun, S. W., Ju, W. K., Lin, S. J., Cross, A. H., & Neufeld, A. H. (2003). Diffusion tensor imaging detects and differentiates axon and myelin degeneration in mouse optic nerve after retinal ischemia. *Neuroimage, 20*, 1714–1722.

Thomas, C., Humphreys, K., Jung, K. J., Minshew, N., & Behrmann, M. (2011). The anatomy of the callosal and visual-association pathways in high-functioning autism: A DTI tractography study. *Cortex, 47*, 863–873.

Tournier, J. D., Mori, S., & Leemans, A. (2011). Diffusion tensor imaging and beyond. *Magnetic Resonance in Medicine, 65*, 1532–1556.

Townsend, J., Courchesne, E., & Egaas, B. (1996). Slowed orienting of covert visual-spatial attention in autism: Specific deficits associated with cerebellar and parietal abnormality. *Development and Psychopathology, 8*, 563–584.

Travers, B. G., Adluru, N., Ennis, C., Tromp do, P. M., Destiche, D., Doran, S., et al. (2012). Diffusion tensor imaging in autism spectrum disorder: A review. *Autism Research, 5*, 289–313.

Vidal, C. N., Nicolson, R., DeVito, T. J., Hayashi, K. M., Geaga, J. A., Drost, D. J., et al. (2006). Mapping corpus callosum deficits in autism: An index of aberrant cortical connectivity. *Biological Psychiatry, 60*, 218–225.

Vigneau, M., Beaucousin, V., Herve, P. Y., Duffau, H., Crivello, F., Houde, O., et al. (2006). Meta-analyzing left hemisphere language areas: Phonology, semantics, and sentence processing. *Neuroimage, 30*, 1414–1432.

Vollm, B. A., Taylor, A. N., Richardson, P., Corcoran, R., Stirling, J., McKie, S., et al. (2006). Neuronal correlates of theory of mind and empathy: A functional magnetic resonance imaging study in a nonverbal task. *Neuroimage, 29*, 90–98.

Waiter, G. D., Williams, J. H., Murray, A. D., Gilchrist, A., Perrett, D. I., & Whiten, A. (2005). Structural white matter deficits in high-functioning individuals with autistic spectrum disorder: A voxel-based investigation. *Neuroimage, 24*, 455–461.

Wakana, S., Caprihan, A., Panzenboeck, M. M., Fallon, J. H., Perry, M., Gollub, R. L., et al. (2007). Reproducibility of quantitative tractography methods applied to cerebral white matter. *Neuroimage, 36*, 630–644.

Whyatt, C. P., & Craig, C. M. (2012). Motor skills in children aged 7–10 years, diagnosed with autism spectrum disorder. *Journal of Autism and Developmental Disorders, 42*, 1799–1809.

Williams, D. L., Cherkassky, V. L., Mason, R. A., Keller, T. A., Minshew, N. J., & Just, M. A. (2013). Brain function differences in language processing in children and adults with autism. *Autism Research,*. doi:10.1002/aur.1291.

Wolff, J. J., Gu, H., Gerig, G., Elison, J. T., Styner, M., Gouttard, S., et al. (2012). Differences in white matter fiber tract development present from 6 to 24 months in infants with autism. *American Journal of Psychiatry, 169*, 589–600.

Wu, Q., Butzkueven, H., Gresle, M., Kirchhoff, F., Friedhuber, A., Yang, Q., et al. (2007). MR diffusion changes correlate with ultra-structurally defined axonal degeneration in murine optic nerve. *Neuroimage, 37*, 1138–1147.

Yendiki, A., Koldewyn, K., Kakunoori, S., Kanwisher, N., & Fischl, B. (2013). Spurious group differences due to head motion in a diffusion MRI study. *Neuroimage, 88C*, 79–90.

Zwarts, M. J., & Guechev, A. (1995). The relation between conduction velocity and axonal length. *Muscle and Nerve, 18*, 1244–1249.

# frontiers in HUMAN NEUROSCIENCE

# Genetic and environmental influences on motor function: a magnetoencephalographic study of twins

**Toshihiko Araki[1], Masayuki Hirata[1,2]\*, Hisato Sugata[2], Takufumi Yanagisawa[1,2], Mai Onishi[1], Yoshiyuki Watanabe[3], Kayoko Omura[4], Chika Honda[4], Kazuo Hayakawa[4] and Shiro Yorifuji[1]**

[1] Division of Functional Diagnostic Science, Osaka University Medical School, Suita, Japan
[2] Department of Neurosurgery, Osaka University Medical School, Suita, Japan
[3] Department of Diagnostic and Interventional Radiology, Osaka University Medical School, Suita, Japan
[4] Center for Twin Research, Osaka University Medical School, Suita, Japan

To investigate the effect of genetic and environmental influences on cerebral motor function, we determined similarities and differences of movement-related cortical fields (MRCFs) in middle-aged and elderly monozygotic (MZ) twins. MRCFs were measured using a 160-channel magnetoencephalogram system when MZ twins were instructed to repeat lifting of the right index finger. We compared latency, amplitude, dipole location, and dipole intensity of movement-evoked field 1 (MEF1) between 16 MZ twins and 16 pairs of genetically unrelated pairs. Differences in latency and dipole location between MZ twins were significantly less than those between unrelated age-matched pairs. However, amplitude and dipole intensity were not significantly different. These results suggest that the latency and dipole location of MEF1 are determined early in life by genetic and early common environmental factors, whereas amplitude and dipole intensity are influenced by long-term environmental factors. Improved understanding of genetic and environmental factors that influence cerebral motor function may contribute to evaluation and improvement for individual motor function.

**Keywords: twins, motor function, movement-related cortical fields, magnetoencephalography**

## INTRODUCTION

Human motor function is attributed by both innate and acquired traits (Lippi et al., 2010; Tucker and Collins, 2012). Innate traits are mainly related to genetic factors, whereas acquired traits are related to environmental factors. Accordingly, although motor function changes with environmental influences such as training, certain genes have been associated with motor function. In particular, the angiotensin converting enzyme (ACE) I allele and the ACTN3 gene (encoding alpha-actinin-3) have been associated with athletic excellence (Gayagay et al., 1998; Yang et al., 2003). Thus in the present study, we hypothesized that cerebral motor function is affected by genetic and environmental influences, based on the assumption that genetically identical brains function differently following long-term exposure to different environments, and reflect brain plasticity. It is important for sports education and training to clarify it. However, little is known to what extent environmental and genetic factors influence cerebral motor function. Middle-aged and elderly monozygotic (MZ) twins are good subjects to investigate the environmental and genetic effects on brain function because a middle-aged and elderly MZ pair is identical with regards to genetic factors but different regarding their environmental exposure. Many studies have compared similarities in electrical brain activity between MZ twins and dizygotic (DZ) twins using electroencephalogram (EEG) and magnetoencephalogram (MEG) (van Beijsterveldt and van Baal, 2002; Smit et al., 2005; Begleiter and Porjesz, 2006; van Pelt et al., 2012). For example, using EEG, the genetic effects on amplitudes and waveforms of several evoked potentials were reported by comparing MZ

twins with DZ twins or unrelated pairs (Lewis et al., 1972). Recently, Van't Ent et al. (2010) revealed genetic influences on waveform amplitude and morphology of entire time series of somatosensory-evoked brain activity in a sample of MZ and DZ twins. However, published twin studies concerning brain activity were limited to primary sensory functions such as visual, auditory, and somatosensory-evoked potentials, and there are no reports to this date on motor-related brain function.

Using MEG, typical responses are observed during voluntary finger movement called movement-related cortical fields (MRCFs) (Cheyne and Weinberg, 1989). MRCFs are representative cortical responses for evaluation of motor function. For example, abnormalities of the time course of MRCFs have been associated with movement disorders such as Parkinson's disease and dystonia (Chen and Hallett, 1999). MRCFs consist of several components, one of which is movement-evoked field 1 (MEF1), which shows the largest and most robust signal (Kristeva et al., 1991; Kristeva-Feige et al., 1995). MEF1 appears approximately 80–120 ms after the onset of muscle contraction (Cheyne and Weinberg, 1989; Cheyne et al., 1997), and the current source underlying MEF1 has been located in primary somatosensory cortex (Cheyne et al., 1997, 2006; Onishi et al., 2006) or primary motor cortex (Onishi et al., 2011). Moreover, peak amplitude of MEF1 increased in Tourette syndrome patients who were characterized by motor tics (Biermann-Ruben et al., 2012), it is considered one of the most important components of MRCFs produced during voluntary movement. In this study, we focused on MEF1 to investigate how genetic and environmental factors affect movement-related brain

activity by evaluating differences between middle-aged and elderly MZ twins and unrelated age-matched pairs.

## MATERIALS AND METHODS

### SUBJECTS

Monozygotic or DZ twins of ≥20 years of age and with no history of neurological or psychiatric episodes were recruited by the Center for Twin Research in Osaka University. We assessed 16 healthy pairs of MZ twins and 15 unrelated individuals (23 males: 65.5 ± 9.5 years; 22 females: 60.3 ± 10.9 years). All subjects were determined to be right-handed by a score in the Edinburgh inventory. Zygosity was determined by short tandem repeat (STR) typing. Written informed consent was obtained from all subjects after explanation of the purpose and possible consequences of the study. This study was approved by the ethics committee of the Osaka University Graduate School of Medicine.

Osaka University Center for Twin Research was organized to collect various information as well as biological resources from registered twins, and to establish a biobank and databases for preserving and managing these data and resources (Hayakawa et al., 2013). The following data are being collected: physical data (e.g., height, body mass, and bone density), data regarding epidemiology (e.g., medical history, lifestyle, cognitive function, and nutrition), EEG, ultrasonography, dentistry, plastic surgery, positron emission tomography, MEG, and magnetic resonance imaging (MRI). In this research, we investigated the cerebral motor function using MEG.
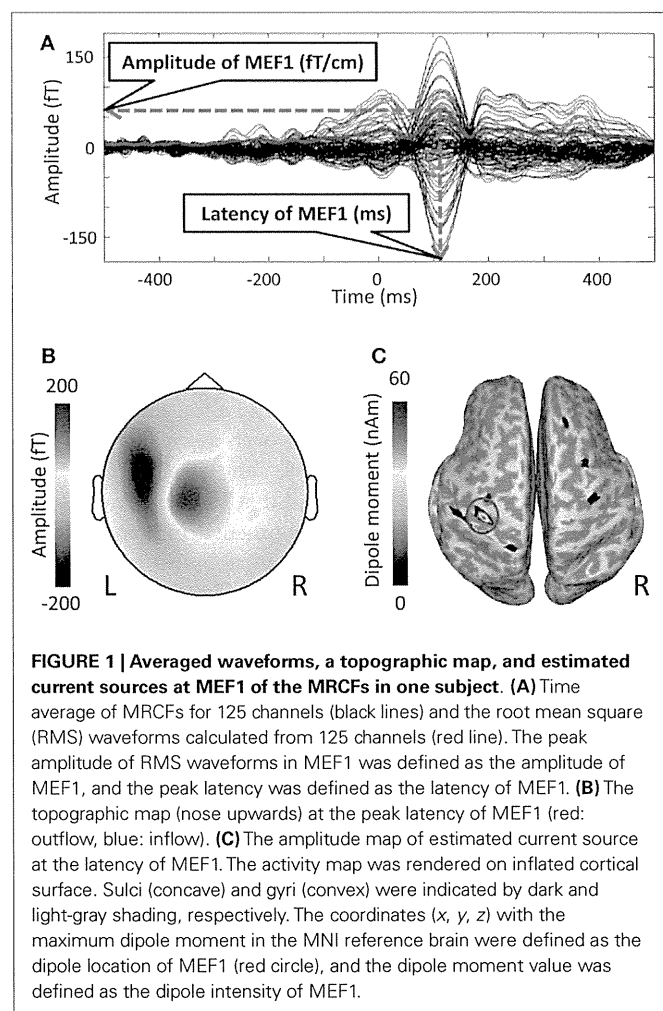
### MEASUREMENTS

The subjects lay on a bed comfortably in the supine position with their head centered into the gantry. They were instructed to close their eyes and to lift the right index finger at self-paced intervals of approximately 5 s. Movements were performed with a very sharp onset, and started from total muscular relaxation. Neuromagnetic activities were recorded in a magnetically shielded room using a 160-channel whole-head MEG system equipped with coaxial type gradiometers (MEG vision NEO; Yokogawa Electric Corporation, Kanazawa, Japan). Data were acquired at a rate of 1000 Hz with an online low-pass filter at 200 Hz. The positions of five head marker coils were obtained before and after recording to localize head position and to evaluate head movement. The maximum acceptable head movement was set at 5 mm and head movements ranged from 0.03 to 3.53 ms. Because head movements were small, the head movement compensation algorithm was not required. Anatomical MRI data were obtained using a 3.0-T magnetic resonance scanner with a standard whole-head coil (Signa HDxt Excite 3.0 T, GE Healthcare UK Ltd., Buckinghamshire, UK).

In order to align MEG data with individual MRI data, we scanned the three-dimensional facial surface of each participant (FastSCAN Cobra, Polhemus, USA). Five head marker coils were attached to the scalp before recording MEG, which provided the position and orientation of MEG sensors relative to the head. Three-dimensional facial surface data were superimposed on the anatomical facial surface provided by the MRI data. We also recorded electromyograms of the right extensor indicis muscle and monitored the self-paced movement of the subjects using two video cameras.

## DATA ANALYSES

The MEG data were analyzed using the standard MEG software of the system (MEG Laboratory; Yokogawa Electric Corporation, Kanazawa, Japan). The onset of each self-paced finger movement was manually determined by an initial rise in the electromyogram waveforms, and this onset time was defined as 0 ms. The time-window of each recoding epochs were defined from −500 to 500 ms. Epochs containing artifacts, such as obvious eye movements and excessive muscle activity were eliminated from the analyses. The epochs were averaged using from −500 to −300 ms as a baseline. Averaged waveforms were high-pass filtered using a cut-off frequency of 1 Hz, and low-pass filtered using a cut-off frequency of 20 Hz. We excluded 35 channels of the bilateral frontal base from the analyses in order to minimize artifact contamination such as eye movement. To determine MEF1, we used the root mean square (RMS), which was calculated from the averaged waveforms of all MEG channels used for analyses (**Figure 1A**). We defined the peak amplitude of MEF1 as the amplitude of MEF1 and the peak latency as the latency of MEF1. We confirmed a clear dipole pattern in the contralateral central region at the peak latency of MEF1 in all subjects (**Figure 1B**).



**FIGURE 1 | Averaged waveforms, a topographic map, and estimated current sources at MEF1 of the MRCFs in one subject. (A)** Time average of MRCFs for 125 channels (black lines) and the root mean square (RMS) waveforms calculated from 125 channels (red line). The peak amplitude of RMS waveforms in MEF1 was defined as the amplitude of MEF1, and the peak latency was defined as the latency of MEF1. **(B)** The topographic map (nose upwards) at the peak latency of MEF1 (red: outflow, blue: inflow). **(C)** The amplitude map of estimated current source at the latency of MEF1. The activity map was rendered on inflated cortical surface. Sulci (concave) and gyri (convex) were indicated by dark and light-gray shading, respectively. The coordinates (x, y, z) with the maximum dipole moment in the MNI reference brain were defined as the dipole location of MEF1 (red circle), and the dipole moment value was defined as the dipole intensity of MEF1.

We also performed dipole source analyses in the peak latency of MEF1 using free software for estimating cortical currents from MEG data (VBMEG; ATR Neural Information Analysis Laboratories, Kyoto, Japan) (Sato et al., 2004; Yoshioka et al., 2008; Toda et al., 2011; Yoshimura et al., 2012). Using each subject's MRI data that was spatially normalized to the Montreal Neurological Institute (MNI) coordinates (Montreal, QC, Canada) using SPM5 (Wellcome Department of Cognitive Neurology, UK)[1], dipole locations of MEFI were calculated on common MNI coordinates. To map current dipoles on the cortical surface, a polygon model of the cortical surface was constructed based on T1-weighted MRI data using FreeSurfer software (Martinos Center software)[2] (Dale et al., 1999; Fischl et al., 1999, 2002). We defined the location on the MNI coordinates of strongest dipole moment around the left central sulci as the dipole location of MEF1 and that of the dipole moment value as the dipole intensity of MEF1 (**Figure 1C**).

In order to evaluate differences in MEF1 between genders, the difference in the average value between males and females was statistically analyzed for the four features of MEFI: latency, amplitude, dipole location, and dipole intensity. To evaluate the differences attributed to age, we sampled the pairs of all the combination from all 47 subjects in such a way that the age difference does not exceed 5 years and computed the correlation coefficients between difference of age and the features of MEF1. Differences in latency, amplitude, and dipole source characteristics (dipole location and intensity) of MEFI were computed for all MZ twin pairs and unrelated age-matched pairs. Unrelated pairs were made by randomly selecting 16 pairs from all subjects without any overlap in pair assignment. Pairs were made such that the age difference may be no more than 5 years.

## RESULTS

Movement-evoked field 1 was consistently observed over the contralateral central region in all subjects. The mean latency of MEF1 was $113.0 \pm 11.5$ ms (mean $\pm$ SD), and the mean amplitude was $45.5 \pm 18.9$ fT/cm. Maximum values of individual differences in latency and amplitude of MEF1 were 48 ms and 78.7 fT/cm, respectively. Mean dipole location at the peak latency of MEF1 was $(-45.3 \pm 5.5, -17.7 \pm 5.7, 60.2 \pm 6.2)$ (MNI coordinates), and mean dipole intensity was $18.9 \pm 13.4$ nAm. There was no statistically significant difference among genders in latency, amplitude, dipole location, and dipole intensity of MEF1 (**Table 1**). All subjects were therefore analyzed independent of gender.

**Figure 2** shows the relationship between difference of age and difference of the features of MEF1 in pairs of all combinations of 47 subjects (312 pairs) such that the age difference may be no more than 5 years. Correlation coefficients for difference of age and difference of the latency, amplitude, dipole location, and dipole intensity were 0.05 ($p = 0.40$; Pearson's correlation test), 0.04 ($p = 0.71$), $-0.03$ ($p = 0.57$), and 0.06 ($p = 0.31$), respectively. No significant correlation was observed in any features.

**Figure 3** shows box and whisker plots of the differences in the latency, amplitude, dipole location, and dipole intensity of MEF1 between MZ twins and unrelated pairs. The average age of all

**Table 1 | Gender differences in MEF1 components.**

| MEF1 components | | Male | Female | *p*\* |
|---|---|---|---|---|
| Latency (ms) | | 113.4 (9.4) | 113.0 (13.9) | 0.903 |
| Amplitude (fT/cm) | | 50.2 (22.2) | 42.9 (13.4) | 0.193 |
| | x coordinate | −45.8 (6.2) | −44.9 (6.6) | 0.631 |
| Dipole location | y coordinate | −18.0 (4.8) | −17.5 (7.1) | 0.756 |
| | z coordinate | 58.2 (7.8) | 61.7 (5.6) | 0.093 |
| Dipole intensity (nAm) | | 18.2 (13.1) | 20.6 (14.6) | 0.569 |

*Values are indicated as means (standard deviation). \*p Values of Student's t-test between male and female subjects.*

16 MZ twins was $62.2 \pm 11.1$ years, and the average age of the corresponding 16 unrelated pairs was $62.8 \pm 10.2$ years. Median values for differences in latency, amplitude, dipole location, and dipole intensity was 2.0 and 14.5 ms, 12.2 and 18.0 fT/cm, 9.0 and 14.0 mm, and 6.7 and 7.2 nAm in MZ twin pairs and unrelated pairs, respectively. Differences in the latency and dipole location among MZ twins were significantly less than those among unrelated pairs (Mann–Whitney $U$ test, $p < 0.05$). However, there were no significant differences in the amplitude and dipole intensity among MZ twin pairs and unrelated pairs.

## DISCUSSION

In this study, we found similarities in the latency and dipole location of MEF1 in MZ twins compared with unrelated pairs. These results indicate that genetic factors and early common environmental factors are dominant for these features of MEF1. Here, we discuss the similarities between MZ twins, particularly factors related to individual differences in the features of MEF1.

The latency of MEF1 in our study showed individual differences of up to 50 ms. A previous study reported that peak latencies of MEF1 ranged from 73.6 to 114 ms (Onishi et al., 2006). The difference among individuals was up to 40.4 ms, which was very similar to the results of our study. In addition, differences of the latency within MZ twins were significantly less than that of unrelated pairs, which means that the latency of MEF1 was similar in MZ twins. Because the average age of MZ twins in this study was >60 years, we assume that long-term differences in the living environments experienced after the MZ twins grew up and lived separately may have caused differences in their brain function. Nevertheless, homogeneity of MEFI latency was preserved even after long-term exposure to different environmental factors. This result indicates that the latency of MEF1 may be strongly affected by genetic and early common environmental factors. Alternatively, MEF1 latency may be affected by nerve conduction velocity, which may reflect myelination. The process of myelination begins early in fetal development and continues systematically for several years (Yakovlev, 1962). In particular, the sensorimotor cortex is involved in the primary myelogenic area, where myelination proceeds from early brain development. Thus, myelination in the sensorimotor cortex may be influenced by genetic and early common environmental factors, and may contribute to the homogeneity of MEF1 latency in the present study. We also found homogeneity in the dipole location in MZ twins. Previous twin studies using MRI reported that strong anatomical similarities were observed in
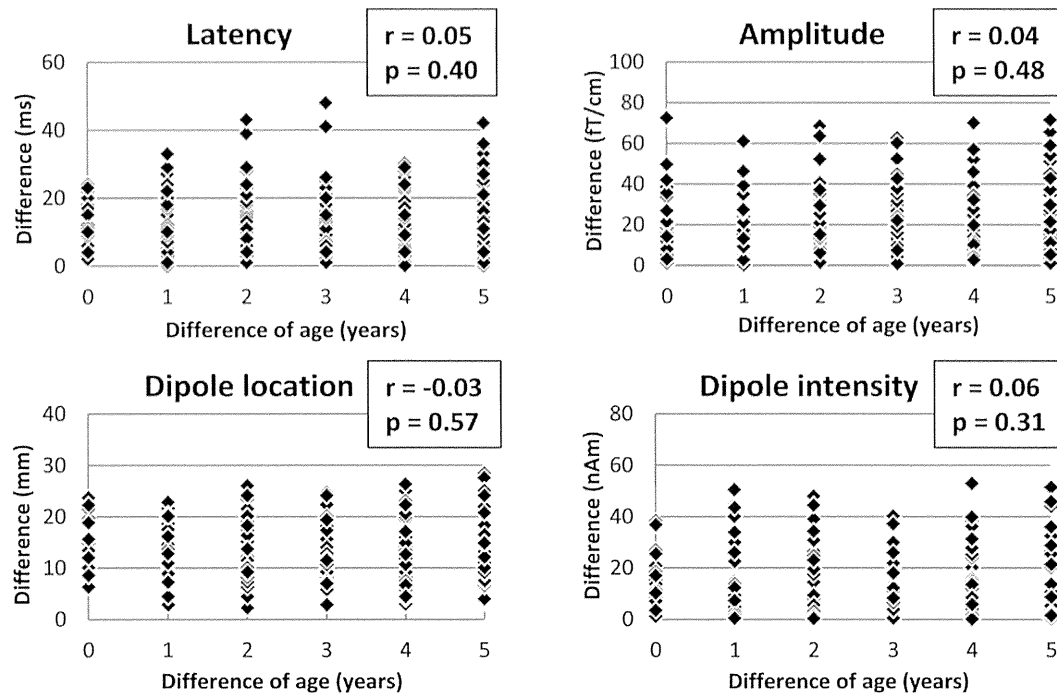
**FIGURE 2 | Scatter diagrams showing the correlation between difference of age and the features of MEF1 in pairs of all combination (312 pairs).** The unrelated pairs were selected in such a way that the age difference did not exceed 5 years. There were no significant correlations between difference of age and each feature (latency, amplitude, dipole moment, dipole intensity) ($p < 0.05$; Pearson's correlation test).
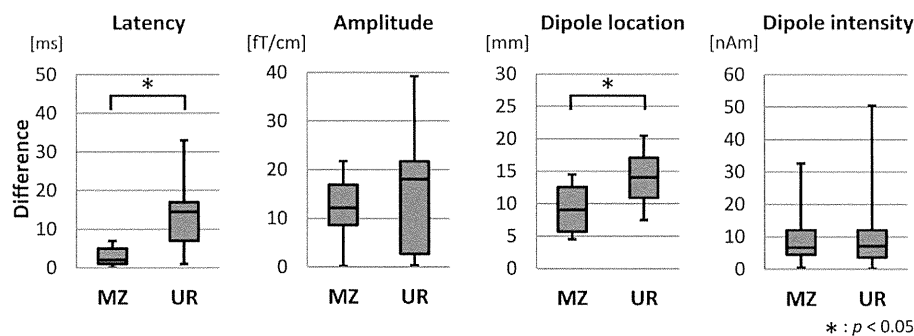


**FIGURE 3 | Box plot diagrams showing the distribution of the features of MEF1 between MZ twin pairs and unrelated pairs.** The lowest and highest lines indicate the lowest and highest data values, respectively. The three lines that form the box indicate 25th, 50th, and 75th percentiles. Differences in the latency and the dipole location of MZ twin pairs were significantly smaller than that between unrelated pairs (Mann–Whitney $U$ test, $p < 0.05$).

frontal and parietal lobes in MZ twins (Eyler et al., 2011, 2012). Taken together, anatomical homogeneity in the frontoparietal area between twins may lead to the similarity of dipole location. Unlike the latency and dipole location of MEF1, we found no significant similarity between amplitude and dipole intensity within MZ twins. The lack of difference in amplitude and dipole intensity between twins and unrelated pairs was likely not a result of the varied movement intensity of individual subjects, but rather that amplitude and dipole intensity of MEF1 are affected by different environmental factors. In previous studies, it has been reported that amplitude and dipole moment of MEF1 does not change even

if finger movement intensity and frequency are changed (Mayville et al., 2005; Onishi et al., 2006). In addition, Van't Ent et al. (2010) reported that amplitude of somatosensory-evoked magnetic field (SEF) is influenced by genetics. SEF induced by electrical nerve stimulation reflects peripheral afferents as well as MEF1. However, SEF reflects cutaneous afferents (Kakigi et al., 2000) while MEF1 reflects sensory feedback from muscle spindle receptors induced by muscle contraction (Oishi et al., 2004). Therefore, physiological differences in the peripheral receptors may be the reason for the difference between MEF1 and SEF. Although individual motor performance was not evaluated in details in the present study, the

sensitivity of muscle spindle changes by strength training (Hakki-nen and Komi, 1983). Taken together, it is suggested that the amplitude of the evoked field from muscle spindles show plasticity and is likely influenced by the individual environmental factors. Specifically, we have demonstrated that MEF1 latency and dipole location are affected by genetic and early common environmental influence, whereas MEF1 amplitude and dipole intensity are affected by long-term individual environmental influences.

The present study is limited to comparisons of MRCFs between MZ and unrelated pairs instead of comparisons between MZ and DZ, which would be ideal for discriminating between genetic and environmental influences. Comparisons of MZ with unrelated pairs fail to decipher genetic from early common environmental influences. However, because middle-aged and elderly subjects have been exposed to individual adulthood environments for sufficiently long times to allow discrimination of these effects from those of genetic and early common environmental influences.

## CONCLUSION

We found that the latency and the current source location of MEF1 were more homogenous between middle-aged and elderly MZ twins than between unrelated pairs, whereas such homogeneity was not found in the amplitude and the current source intensity of MEF1. These results suggest that some of the basic neurophysiological factors of cerebral motor function are determined early in life by genetic and early common environmental factors, while others are influenced by long-term environmental factors. These data improve the understanding of genetic and environmental factors that influence cerebral motor function and may contribute to assessments of individual motor function.

## ACKNOWLEDGMENTS

## REFERENCES

Begleiter, H., and Porjesz, B. (2006). Genetics of human brain oscillations. Int. J. Psychophysiol. 60, 162–171. doi:10.1016/j.ijpsycho.2005.12.013

Biermann-Ruben, K., Miller, A., Franzkowiak, S., Finis, J., Pollok, B., Wach, C., et al. (2012). Increased sensory feedback in Tourette syndrome. Neuroimage 63, 119–125. doi:10.1016/j.neuroimage.2012.06.059

Chen, R., and Hallett, M. (1999). The time course of changes in motor cortex excitability associated with voluntary movement. Can. J. Neurol. Sci. 26, 163–169.

Cheyne, D., Bakhtazad, L., and Gaetz, W. (2006). Spatiotemporal mapping of cortical activity accompanying voluntary movements using an event-related beamforming approach. Hum. Brain Mapp. 27, 213–229. doi:10.1002/hbm.20178

Cheyne, D., Endo, H., Takeda, T., and Weinberg, H. (1997). Sensory feedback contributes to early movement-evoked fields during voluntary finger movements in humans. Brain Res. 771, 196–202. doi:10.1016/S0006-8993(97)00765-8

Cheyne, D., and Weinberg, H. (1989). Neuromagnetic fields accompanying unilateral finger movements: pre-movement and movement-evoked fields. Exp. Brain Res. 78, 604–612. doi:10.1007/BF00230248

Dale, A. M., Fischl, B., and Sereno, M. I. (1999). Cortical surface-based analysis. I. Segmentation and surface reconstruction. Neuroimage 9, 179–194. doi:10.1006/nimg.1998.0395

Eyler, L. T., Chen, C. H., Panizzon, M. S., Fennema-Notestine, C., Neale, M. C., Jak, A., et al. (2012). A comparison of heritability maps of cortical surface area and thickness and the influence of adjustment for whole brain measures: a magnetic resonance imaging twin study. Twin Res. Hum. Genet. 15, 304–314. doi:10.1017/thg.2012.3

Eyler, L. T., Prom-Wormley, E., Panizzon, M. S., Kaup, A. R., Fennema-Notestine, C., Neale, M. C., et al. (2011). Genetic and environmental contributions to regional cortical surface area in humans: a magnetic resonance imaging twin study. Cereb. Cortex 21, 2313–2321. doi:10.1093/cercor/bhr013

Fischl, B., Salat, D. H., Busa, E., Albert, M., Dieterich, M., Haselgrove, C., et al. (2002). Whole brain segmentation: automated labeling of neuroanatomical structures in the human brain. Neuron 33, 341–355. doi:10.1016/S0896-6273(02)00569-X

Fischl, B., Sereno, M. I., and Dale, A. M. (1999). Cortical surface-based analysis. II: inflation, flattening, and a surface-based coordinate system. Neuroimage 9, 195–207. doi:10.1006/nimg.1998.0396

Gayagay, G., Yu, B., Hambly, B., Boston, T., Hahn, A., Celermajer, D. S., et al. (1998). Elite endurance athletes and the ACE I allele – the role of genes in athletic performance. Hum. Genet. 103, 48–50. doi:10.1007/s004390050781

Hakkinen, K., and Komi, P. V. (1983). Changes in neuromuscular performance in voluntary and reflex contraction during strength training in man. Int. J. Sports Med. 4, 282–288. doi:10.1055/s-2008-1026051

Hayakawa, K., Iwatani, Y., and Osaka Twin Research, G. (2013). An overview of multidisciplinary research resources at the Osaka University Center for Twin Research. Twin Res. Hum. Genet. 16, 217–220. doi:10.1017/thg.2012.141

Kakigi, R., Hoshiyama, M., Shimojo, M., Naka, D., Yamasaki, H., Watanabe, S., et al. (2000). The somatosensory evoked magnetic fields. Prog. Neurobiol. 61, 495–523. doi:10.1016/S0301-0082(99)00063-5

Kristeva, R., Cheyne, D., and Deecke, L. (1991). Neuromagnetic fields accompanying unilateral and bilateral voluntary movements: topography and analysis of cortical sources. Electroencephalogr. Clin. Neurophysiol. 81, 284–298. doi:10.1016/0168-5597(91)90015-P

Kristeva-Feige, R., Rossi, S., Pizzella, V., Tecchio, F., Romani, G. L., Erne, S., et al. (1995). Neuromagnetic fields of the brain evoked by voluntary movement and electrical stimulation of the index finger. Brain Res. 682, 22–28. doi:10.1016/0006-8993(95)00313-F

Lewis, E. G., Dustman, R. E., and Beck, E. C. (1972). Evoked response similarity in monozygotic, dizygotic and unrelated individuals: a comparative study. Electroencephalogr. Clin. Neurophysiol. 32, 309–316. doi:10.1016/0013-4694(72)90180-0

Lippi, G., Longo, U. G., and Maffulli, N. (2010). Genetics and sports. Br. Med. Bull. 93, 27–47. doi:10.1093/bmb/ldp007

Mayville, J. M., Fuchs, A., and Kelso, J. A. (2005). Neuromagnetic motor fields accompanying self-paced rhythmic finger movement at different rates. Exp. Brain Res. 166, 190–199. doi:10.1007/s00221-005-2354-2

Oishi, M., Kameyama, S., Fukuda, M., Tsuchiya, K., and Kondo, T. (2004). Cortical activation in area 3b related to finger movement: an MEG study. Neuroreport 15, 57–62. doi:10.1097/00001756-200401190-00012

Onishi, H., Oyama, M., Soma, T., Kirimoto, H., Sugawara, K., Murakami, H., et al. (2011). Muscle-afferent projection to the sensorimotor cortex after voluntary movement and motor-point stimulation: an MEG study. Clin. Neurophysiol. 122, 605–610. doi:10.1016/j.clinph.2010.07.027

Onishi, H., Soma, T., Kameyama, S., Oishi, M., Fuijmoto, A., Oyama, M., et al. (2006). Cortical neuromagnetic activation accompanying two types of voluntary finger extension. Brain Res. 1123, 112–118. doi:10.1016/j.brainres.2006.09.033

Sato, M. A., Yoshioka, T., Kajihara, S., Toyama, K., Goda, N., Doya, K., et al. (2004). Hierarchical Bayesian estimation for MEG inverse problem. Neuroimage 23, 806–826. doi:10.1016/j.neuroimage.2004.06.037

Smit, D. J., Posthuma, D., Boomsma, D. I., and Geus, E. J. (2005). Heritability of background EEG across the power spectrum. Psychophysiology 42, 691–697. doi:10.1111/j.1469-8986.2005.00352.x

Toda, A., Imamizu, H., Kawato, M., and Sato, M. A. (2011). Reconstruction of two-dimensional movement trajectories from selected magnetoencephalography cortical currents by combined sparse Bayesian methods. Neuroimage 54, 892–905. doi:10.1016/j.neuroimage.2010.09.057

Tucker, R., and Collins, M. (2012). What makes champions? A review of the relative contribution of genes and training to sporting success. Br. J. Sports Med. 46, 555–561. doi:10.1136/bjsports-2011-090548

van Beijsterveldt, C. E., and van Baal, G. C. (2002). Twin and family studies of the human electroencephalogram: a review and a meta-analysis. Biol. Psychol. 61, 111–138. doi:10.1016/S0301-0511(02)00055-8

van Pelt, S., Boomsma, D. I., and Fries, P. (2012). Magnetoencephalography in twins reveals a strong genetic determination of the peak frequency of visually induced gamma-band synchronization. J. Neurosci. 32, 3388–3392. doi:10.1523/JNEUROSCI.5592-11.2012

Van't Ent, D., Van Soelen, I. L., Stam, K. J., De Geus, E. J., and Boomsma, D. I. (2010). Genetic influence demonstrated for MEG-recorded somatosensory evoked responses. *Psychophysiology* 47, 1040–1046. doi:10.1111/j.1469-8986.2010.01012.x

Yakovlev, P. I. (1962). Morphological criteria of growth and maturation of the nervous system in man. *Res. Publ. Assoc. Res. Nerv. Ment. Dis.* 39, 3–46.

Yang, N., Macarthur, D. G., Gulbin, J. P., Hahn, A. G., Beggs, A. H., Easteal, S., et al. (2003). ACTN3 genotype is associated with human elite athletic performance. *Am. J. Hum. Genet.* 73, 627–631. doi:10.1086/377590

Yoshimura, N., Dasalla, C. S., Hanakawa, T., Sato, M. A., and Koike, Y. (2012). Reconstruction of flexor and extensor muscle activities from electroencephalography cortical currents. *Neuroimage* 59, 1324–1337. doi:10.1016/j.neuroimage.2011.08.029

Yoshioka, T., Toyama, K., Kawato, M., Yamashita, O., Nishina, S., Yamagishi, N., et al. (2008). Evaluation of hierarchical Bayesian method through retinotopic brain activities reconstruction from fMRI and MEG signals. *Neuroimage* 42, 1397–1413. doi:10.1016/j.neuroimage.2008.06.013

# Cerebral Aneurysm Pulsation: Do Iterative Reconstruction Methods Improve Measurement Accuracy In Vivo?

T. Illies, D. Säring, M. Kinoshita, T. Fujinaka, M. Bester, J. Fiehler, N. Tomiyama, and Y. Watanabe

## ABSTRACT

**BACKGROUND AND PURPOSE:** Electrocardiogram-gated 4D-CTA is a promising technique allowing new insight into aneurysm pathophysiology and possibly improving risk prediction of cerebral aneurysms. Due to the extremely small pulsational excursions (<0.1 mm in diameter), exact segmentation of the aneurysms is of critical importance. In vitro examinations have shown improvement of the accuracy of vessel delineation by iterative reconstruction methods. We hypothesized that this improvement shows a measurable effect on aneurysm pulsations in vivo.

**MATERIALS AND METHODS:** Ten patients with cerebral aneurysms underwent 4D-CTA. Images were reconstructed with filtered back-projection and iterative reconstruction. The following parameters were compared between both groups: image noise, absolute aneurysm volumes, pulsatility, and sharpness of aneurysm edges.

**RESULTS:** In iterative reconstruction images, noise was significantly reduced (mean, $9.8 \pm 4.0$ Hounsfield units versus $8.0 \pm 2.5$ Hounsfield units; $P = .04$), but the sharpness of aneurysm edges just missed statistical significance (mean, $3.50 \pm 0.49$ mm versus $3.42 \pm 0.49$ mm; $P = .06$). Absolute volumes (mean, $456.1 \pm 775.2$ mm$^3$ versus $461.7 \pm 789.9$ mm$^3$; $P = .31$) and pulsatility (mean, $1.099 \pm 0.088$ mm$^3$ versus $1.095 \pm 0.082$ mm$^3$; $P = .62$) did not show a significant difference between iterative reconstruction and filtered back-projection images.

**CONCLUSIONS:** CT images reconstructed with iterative reconstruction methods show a tendency toward shorter vessel edges but do not affect absolute aneurysm volumes or pulsatility measurements in vivo.

**ABBREVIATIONS:** AIDR = adaptive iterative dose reduction; IR = iterative reconstruction; FBP = filtered back-projection; HU = Hounsfield units

E lectrocardiogram-gated 4D-CT angiography has been used to analyze the pulsation of cerebral aneurysms.[1-7] Insight into aneurysm pathophysiology and improvement of risk prediction of incidental cerebral aneurysms can be expected. The technique is limited by the small pulsational excursions of cerebral aneurysms. If one considers a volume change of 5% within the cardiac cycle, the change in diameter of a spherical aneurysm of 5 mm diameter is on the order of 0.1 mm,[1,2] which is below the resolution of CTA. Exact segmentation of the aneurysm is, therefore, critical and of the utmost importance for the correct analysis of pulsations.

In vitro experiments with vascular models have shown that vessel delineation depends on various factors, including intraluminal contrast attenuation, vascular wall thickness, postprocessing, and reconstruction methods.[8] Iterative reconstruction (IR) algorithms have gained importance in clinical routine CT because the radiation dose can be reduced significantly while image quality is maintained compared with filtered back-projection (FBP) reconstruction. At a constant radiation dose, IR reduces image blur, enhances edges, and increases image resolution.[8-10] Depiction of vessels in the posterior fossa and the spinal canal[11,12] is improved in vivo. Moreover, in vitro studies reveal improvement of the accuracy of quantitative measurement of vessel diameters.[8]

These findings and its overall characteristics make IR an interesting tool for improving the accuracy of pulsation measurements of cerebral aneurysms. To our knowledge, the influence of IR on vessel-volume measurement, especially in 4D-CTA, has not been examined in vivo. We hypothesized that IR methods have a measureable effect on the accuracy of quantification of cerebral aneurysm pulsation in vivo.

## MATERIALS AND METHODS

### Patients

Ten patients with unruptured cerebral aneurysms underwent 4D-CTA. Four aneurysms were located at the internal carotid artery; 4, at the middle cerebral artery; 1, at the anterior communicating artery; and 1, at the anterior cerebral artery. The local ethics committee approved the use of the clinical data for research and waived the requirement for written informed consent from patients. Patient data are listed in the Table.

### 4D-CTA Acquisition

Retrospectively electrocardiogram-gated CTA was performed on a 320-detector row Aquilion ONE CT scanner (Toshiba Medical Systems, Tokyo, Japan). We used the following parameters: 120-kV tube voltage, 270-mA tube current, 350-ms gantry rotation time, 140-mm z-coverage. Contrast medium (ioversol, Optiray 320 mg I/mL; Covidien Japan, Tokyo, Japan) was injected at 5 mL/s. Timing for the image aquisition was determined with a test injection of 15 mL of contrast medium. For CTA, 50 mL of contrast medium was injected followed by a saline flush. 4D-CTAs were reconstructed with half reconstruction by using FBP and a kernel optimized for intracranial vessel imaging and IR

algorithm (adaptive iterative dose reduction [AIDR] 3D) with 10 steps of each 10% of the R-R interval, 512 × 512 image matrix, 0.5-mm section thickness, and 0.39 × 0.39 mm in-plane resolution.

### Postprocessing

We used an in-house-developed software as well as ImageJ software (National Institutes of Health, Bethesda, Maryland) and MeVisLab (MeVis Medical Solutions, Bremen, Germany) for volume measurement, and R (http://www.r-project.org/) and R Studio 0.97 (http://rstudio.org/download/desktop) for statistical analysis.

### Noise

Mean and SDs were calculated from circular ROIs in air (400 mm$^2$), brain tissue (200 mm$^2$), and the aneurysm on transversal sections in all phases in FBP and AIDR images. The SDs of the densities within the ROIs were averaged over all timeframes, and their means and SDs were compared between the FBP and AIDR images with $t$ tests as a measure of objective image noise.

### Edge Sharpness

For each aneurysm, 1 attenuation profile along a line passing through its center was acquired on axial images. Measurement points were interpolated by using cubic splines. The width of the edge response of the aneurysm wall was defined as the distance between points corresponding to 10% and 90% of the maximum intra-aneurysmal attenuation on the border of the aneurysms. A shorter edge response corresponds to a sharper edge representation. Edge responses were compared between FBP and IR groups (Fig 1).

### Absolute Volumes and Pulsatility

Datasets were loaded into an in-house-developed postprocessing software. Perivascular tissue was removed with a thresholded segmentation (160–

**Patient characteristics**

| Patient No. | Age (yr) | Location (Artery) | Volume (mm3)[a] AIDR | Volume (mm3)[a] FBP | Diameter (mm)[b] |
|---|---|---|---|---|---|
| 1 | 53 | MCA | 2336.4 | 2386.0 | 16.7 |
| 2 | 66 | AcomA | 95.1 | 95.7 | 6.1 |
| 3 | 55 | ICA | 69.1 | 72.9 | 5.7 |
| 4 | 70 | MCA | 15.3 | 15.4 | 3.9 |
| 5 | 50 | ICA | 1352.5 | 1361.7 | 15.1 |
| 6 | 69 | ACA | 67.4 | 67.3 | 4.3 |
| 7 | 61 | ICA | 76.7 | 77.2 | 5.9 |
| 8 | 76 | MCA | 58.6 | 59.2 | 5.7 |
| 9 | 50 | ICA | 408.8 | 407.1 | 10.7 |
| 10 | 68 | MCA | 82.2 | 74.4 | 7.1 |

**Note:**—AcomA indicates anterior communicating artery; ACA, anterior cerebral artery.
[a] For volume measurement, a 3D model of the vasculature was created and the aneurysms were interactively segmented (see "Material and Methods" section).
[b] The aneurysm diameter is the maximum value of the axial, coronal, or sagittal aneurysm diameter.
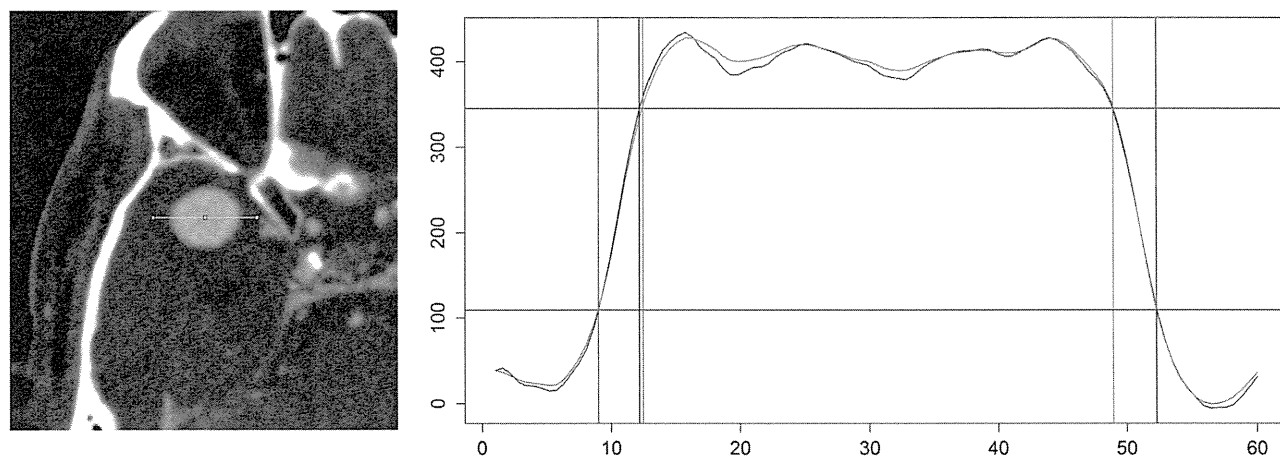


**FIG 1.** Creation of a line profile across the aneurysms for calculations of edge lengths. The left side shows a right middle cerebral artery aneurysm. A linear region of interest is positioned through the center of the aneurysm. The right side shows a cubic spline function fitted to the measurements for FBP (black) and AIDR (red). Edges are defined as the distance between the 10% and 90% interval of the maximum intra-aneurysmal attenuation (*horizontal black lines*).